microscope (Olympus, Tokyo, Japan) or an All-in-One BZ-9000 Fluorescence microscope (KEYENCE, Osaka, Japan). Digital image Z-stacks were created, and projections were made from them using an Olympus FV1000 microscope and FV10-ASW software (Olympus). Fluorescence intensity was measured using the NIH Image J Program.

2.5. Quantification of cellular Purkinje cell size

Sixteen-micrometer stacks of cerebellar optical sections were collected using an All-in-One BZ-9000 Fluorescence microscope and Z-stack images were joined into sagittal images using BZ-II software (KEYENCE). These data were transferred into Neurolucida software (MBF Bioscience, Japan, Inc., Chiba, Japan). Four stacks (each 0.09 μm^2 in area) for each of three sections from WT, HGF-Tg, SCA7-KI, and SCA7-KI/HGF-Tg mice ($n = 3$ each) were used to measure the cell sizes of calbindin-positive Purkinje cells. Quantification of cell size was performed as previously described with slight modifications (Yoo et al., 2003). Briefly, each cell surface was outlined manually. The perikaryon area of each cell was estimated to be the approximately circular area enclosed by the cell perimeter and the extension of the cell perimeter toward the initial point of dendrite extension. Partial cells and binary cell images were excluded based upon cell shape and relative fluorescence intensity.

2.6. Enzyme-linked immunosorbent assay (ELISA)

After the mice were placed under deep anesthesia with an overdose of sodium pentobarbital, the cerebella of WT, HGF-Tg, SCA7-KI, and SCA7-KI/HGF-Tg mice ($n = 4$ each) were collected, quickly frozen and stored at −80 °C until used. Frozen tissue samples were homogenized, subsequently sonicated using a Bioruptor UCD-250 (Cosmo Bio Co., Ltd., Tokyo, Japan), and centrifuged at 4 °C. The supernatants were then used to quantify HGF protein levels using ELISA (Institute of Immunology Co., Ltd., Tokyo, Japan) as previously described (Kadoyama et al., 2007; Sun et al., 2002; Yamada et al., 1995).

2.7. Assessment of motor performance

A rotarod apparatus (Bioseb, Paris, France) was used to assess the ability of an animal to balance on an elevating rotating metal rod (Carter et al., 2001). Rotarod tests are a common tool of studies of mouse models of spinocerebellar ataxia (Yoo et al., 2003; Custer et al., 2006). In this study, 10-week-old mice (WT; $n = 13$, HGF-Tg; $n = 12$, SCA7-KI; $n = 12$, SCA7-KI/HGF-Tg; $n = 8$) were placed on the rotarod, the speed of which was set at 5 rpm initially and accelerated until reaching a speed of 20 rpm for 5 min. After taking a rest for more than 5 min, the latency to fall from the rotarod was measured for 5 min using the machine mode (initial rate of 5 rpm; acceleration until reaching 40 rpm for 10 min). The average latency to fall for each genotype was calculated.

2.8. Statistical analyses

Statistical analyses were carried out using StatView software version 5.0.1 (SAS institute, Cary, NC). Differences in the total intensities of immunostaining for HGF, GLAST, GLT1, size of Purkinje cells, and regional HGF levels in the cerebellum among the above animal models were all determined by one-way ANOVA with Fisher's PLSD tests. Latency to fall in rotarod tests was analyzed using the Student's t-test. The results are presented as the mean ± S.E.M. A value of $P < 0.05$ was considered statistically significant.

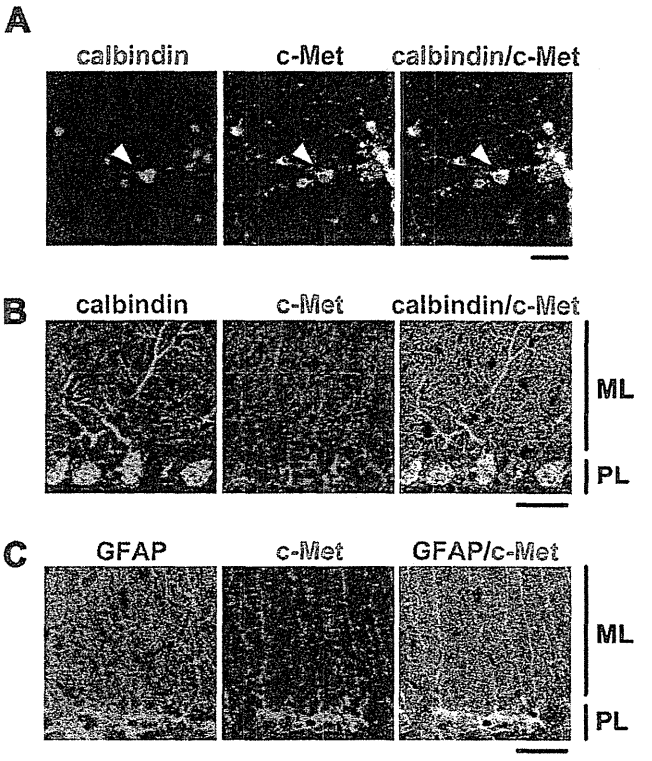

Fig. 1. Immunocytochemical and immunohistochemical localization of c-Met in cerebellar cells *in vitro* and *in vivo*. HGF receptor (c-Met) is expressed in Purkinje cells of the mouse cerebellum *in vitro* and *in vivo*. (A) Immunocytochemistry in primary neuronal cultures of the cerebellum from E16 mouse embryos. Purkinje cells show double immunoreactivity (white arrowheads) for calbindin (red) and c-Met (green) in culture. Bar, 30 μm. (B and C) Immunohistochemistry in 10-week-old wild-type (WT) mice. (B) Purkinje cells show double immunoreactivity against calbindin (green) and c-Met (red). PL, Purkinje cell layer; ML, molecular layer. Bar, 30 μm. (C) Bergmann glia show double immunoreactivity against GFAP (green) and c-Met (red). Bar, 30 μm. (For interpretation of the references to color in this figure caption, the reader is referred to the web version of the article.)

3. Results

3.1. c-Met is expressed in the cerebellar Purkinje cells in vitro

To assess whether cerebellar Purkinje cells are potential target cells of HGF, we first performed double immunostaining of c-Met (green) and calbindin (red), a marker for Purkinje cells, in primary cultures of embryonic mouse cerebellar neurons *in vitro*. c-Met-immunoreactivity (IR) was observed in a large number of cerebellar neurons, with most of these presumably being granular cells. In addition to these neurons, c-Met-IR was indeed detected in calbindin-positive Purkinje cells (Fig. 1A).

3.2. c-Met is expressed in the cerebellar Purkinje cells and Bergmann glia in vivo

We next assessed whether c-Met is expressed in Purkinje cells *in vivo* using double immunostaining for c-Met (red) and calbindin (green) in the cerebella of WT mice. c-Met-IR was detected in Purkinje cells of the cerebella of WT mice. In addition, c-Met-IR was detected in other cells surrounding to the Purkinje cells (Fig. 1B). These cells that were closely apposed to Purkinje cells resembled Bergmann glia. To determine if these non-Purkinje cells were Bergmann glia, double immunostaining for c-Met (red) and GFAP (green), a marker for Bergmann glia, was performed. As shown in Fig. 1C, c-Met-IR was detected in Bergmann glia. These findings

Please cite this article in press as: Noma, S., et al., Overexpression of HGF attenuates the degeneration of Purkinje cells and Bergmann glia in a knockin mouse model of spinocerebellar ataxia type 7. Neurosci. Res. (2012), doi:10.1016/j.neures.2012.03.001

indicate that both Purkinje cells and Bergmann glia are potential target cells of HGF *in vivo*.

3.3. Immunohistochemical analyses of HGF and phospho-c-Met in the cerebellum of WT, HGF-Tg, SCA7-KI, and SCA7-KI/HGF-Tg mice

To explore whether HGF can modify the degeneration of Purkinje cells in SCA7-KI mice, we used neuron-specific enolase (NSE)-driven HGF overexpression transgenic mice (HGF-Tg) to introduce HGF into the Purkinje cells of SCA7-KI mice. Crossing SCA7-KI mice with HGF-Tg mice generated the following four mouse models: (1) wild-type littermates (WT), (2) HGF-Tg, (3) SCA7-KI, and (4) SCA7-KI/HGF-Tg mice. This approach allowed the stable introduction of the HGF gene directly into the cerebellar neurons of SCA7-KI mice. Confirmation that HGF was introduced into the cerebellum of SCA7-KI/HGF-Tg mice was accomplished with immunostaining. HGF-IR was faintly detected in calbindin-positive Purkinje cells and GFAP-positive Bergman glia of the cerebellum in WT and SCA7-KI mice (Fig. 2A, upper panel), while more intense staining of HGF-IR was detected in Purkinje cells of HGF-Tg mice as well as in SCA7-KI/HGF-Tg mice (Fig. 2A, bottom panel). In addition to Purkinje cells, HGF-IR was detected in cells surrounding the Purkinje cells, *i.e.* GFAP-positive Bergmann glia. These findings were further confirmed by quantitative analyses of the immunofluorescent intensity of HGF-IR in sections of the cerebellum (Fig. 2B) and HGF content using ELISA analyses (Fig. 2C). These findings suggest that overexpressed HGF in cerebellar neurons is released into the extracellular space, and is in turn distributed to Bergmann glia.

3.4. c-Met is tyrosine-phosphorylated in Purkinje cells and Bergmann glia in SCA7-KI/HGF-Tg mice

Further attempts were made to determine if overexpression of HGF contributes to tyrosine-phosphorylation, and thereby activation, of c-Met in SCA7-KI/HGF-Tg mice. The level of phospho-c-Met-IR was much higher in both the Purkinje cells and Bergmann glia of SCA7-KI/HGF-Tg mice compared to those of SCA7-KI mice. These findings demonstrate that overexpression of HGF in SCA7-KI/HGF-Tg mice contributes to the activation of c-Met in Purkinje cells and Bergmann glia, prompting an examination of the role of HGF in the modulation of these cells in SCA7-KI mice (Fig. 2D).

3.5. Overexpression of HGF attenuates the degeneration of Purkinje cells of the cerebellum in SCA7-KI mice

To elucidate whether HGF plays a role in attenuating the degeneration of Purkinje cells in SCA7-KI mice, we next compared the morphology of Purkinje cells from the cerebella of SCA7-KI and SCA7-KI/HGF-Tg mice. Calbindin immunohistochemistry revealed that Purkinje cells appeared to have large spherical cell bodies in both WT and HGF-Tg mice, while a number of Purkinje cells with reduced cellular size (degenerated neurons, white arrowheads), were present in SCA7-KI mice (Fig. 3A). In contrast, many more large spherical neurons were observed in SCA7-KI/HGF-Tg mice compared to SCA7-KI mice (Fig. 3A). The size distribution of Purkinje cells in WT, HGF-Tg, SCA7-KI, and SCA7-KI/HGF-Tg mice is shown in Fig. 3B. Quantitative analyses showed that the size of Purkinje cells in SCA7-KI mice was varied from small (<150 μm^2) to large (>150 μm^2; healthy), while the quantity of small Purkinje cells (<150 μm^2) was reduced in SCA7-KI/HGF-Tg mice (Fig. 3B). Namely, the fraction of small Purkinje cells was significantly lower in SCA7-KI/HGF-Tg mice than in SCA7-KI mice. These findings demonstrate that overexpression of HGF attenuates the degeneration of Purkinje cells in SCA7-KI mice.

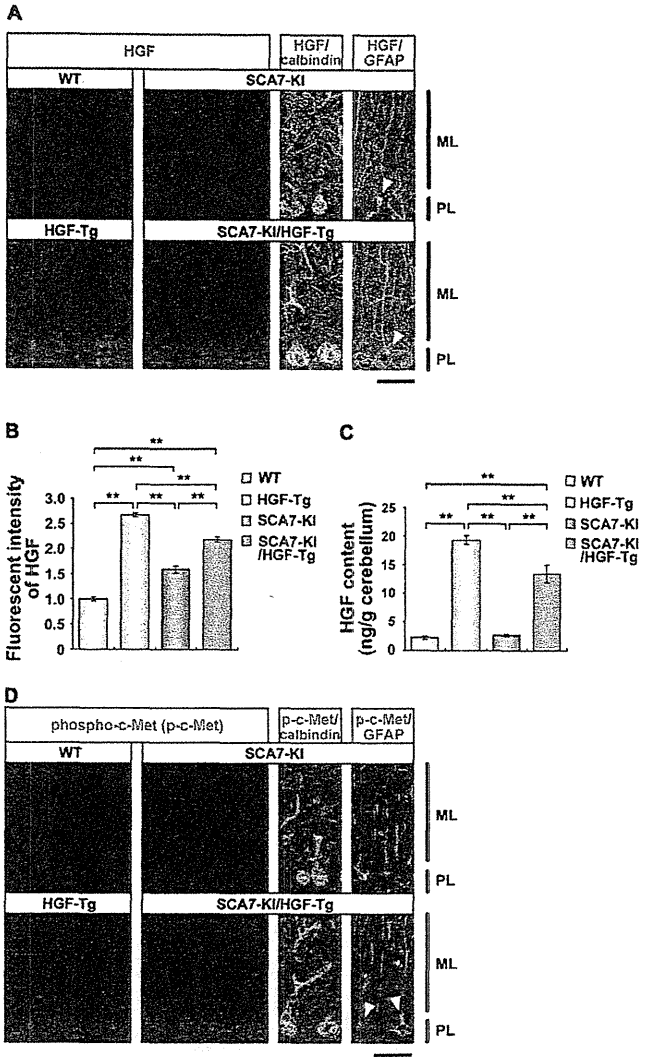

Fig. 2. Immunohistochemical localization of HGF and phospho-c-Met in cerebellar cells *in vivo*. Comparison of HGF levels by immunohistochemistry (A and B) and HGF ELISA (C) in the cerebellum of 10-week-old WT, HGF-Tg, SCA7-KI, and SCA7-KI/HGF-Tg mice using anti-rat HGF that detects both endogenous and exogenous (overexpressed) HGF proteins. (A) HGF-IR is elevated in HGF-Tg and SCA7-KI/HGF-Tg mice. PL, Purkinje cell layer; ML, molecular layer. Bar, 30 μm. White arrowhead indicates GFAP/HGF double-positive cells. (B) Fluorescent intensity ($n = 6$ per group) of HGF in each group. Mean HGF signal intensity was significantly elevated compared to WT (**$P < 0.01$, Fisher's PLSD test). Error bars indicate S.E.M. (C) HGF protein levels in the whole cerebellum are elevated in HGF-Tg and SCA7-KI/HGF-Tg mice ($n = 4$ per group, **$P < 0.01$, Fisher's PLSD test). Error bars indicate S.E.M. (D) Immunohistochemistry of tyrosine phosphorylation at positions 1230, 1234, and 1235 of c-Met (phospho-c-Met, red) in the cerebellum in 10-week-old mice. Phospho-c-Met staining is shown in the cerebellum in all mice groups. Phospho-c-Met-IR is elevated in both Purkinje cells (lower left panel, green) and Bergmann glia (lower right panel, green) of SCA7-KI/HGF-Tg mice compared to SCA7-KI mice (upper panel, green). White arrowheads indicate GFAP/phospho-c-Met double-positive cells. Bar, 30 μm. (For interpretation of the references to color in this figure caption, the reader is referred to the web version of the article.)

3.6. Overexpression of HGF maintains the levels of the glutamate transporters (GLAST and GLT-1) in the cerebellum of SCA7-KI mice

Bergmann glia are responsible for glutamate uptake (removal) from the Purkinje cell synaptic cleft. It has been suggested that polyglutamine-expanded ataxin-7 induces Purkinje cell excitotoxicity by interfering with Bergmann glia-mediated glutamate uptake. This is due to the fact that the expression of GLAST, a

Please cite this article in press as: Noma, S., et al., Overexpression of HGF attenuates the degeneration of Purkinje cells and Bergmann glia in a knockin mouse model of spinocerebellar ataxia type 7. Neurosci. Res. (2012), doi:10.1016/j.neures.2012.03.001

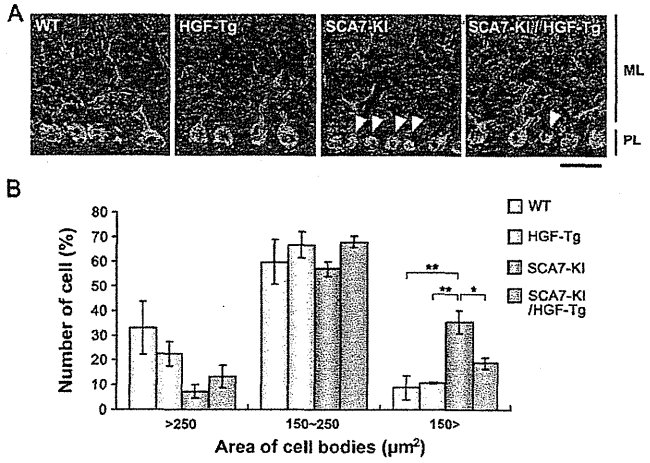

Fig. 3. HGF attenuates degeneration of Purkinje cell bodies. (A) Immunohistochemistry of calbindin (green) in the cerebellum of 10-week-old mice. SCA7-KI mice displayed smaller Purkinje cell body size than WT and HGF-Tg mice. SCA7-KI/HGF-Tg mice showed an attenuation of shrinkage of Purkinje cell bodies. PL, Purkinje cell layer; ML, molecular layer. Bar, 30 μm. White arrowhead indicates degenerative Purkinje cell changes. (B) Quantification of cell numbers with different Purkinje cellular body size (>250; 150–250; <150 μm^2) of each group ($n = 3$ per group). The number of small cells (area are less than 150 μm^2) in SCA7-KI mice is significantly greater *versus* WT and HGF-Tg mice (**$P < 0.01$, Fisher's PLSD test), SCA7-KI/HGF-Tg mice exhibit significantly fewer small cells compared to SCA7-KI mice (*$P < 0.05$). Error bars indicate S.E.M. (For interpretation of the references to color in this figure caption, the reader is referred to the web version of the article.)

glutamate transporter in the cerebellum, is confined to Bergmann glia and marked reductions in GLAST expression (and glutamate uptake) have been observed in presymptomatic Gfa2-SCA7-92Q mice (Custer et al., 2006). As c-Met is expressed in the Bergmann glia of WT mice and is phosphorylated (*i.e.* activated) in Bergmann glia in SCA7-KI/HGF-Tg mice (Figs. 1C and 2D), we next examined whether HGF affects the morphology and function of Bergmann glia. Immunostaining for GFAP revealed that obvious morphological difference of Bergmann glia was not detected between WT mice and SCA7-KI/HGF-Tg mice (Fig. 4A). We then examined whether HGF modulates the down-regulation of GLAST levels in SCA7-KI mice. Immunostaining for GLAST revealed that GLAST levels were decreased in SCA7-KI mice compared to WT mice, while the levels were generally maintained in SCA7-KI/HGF-Tg mice (Fig. 4B and C). These findings demonstrate that HGF supports GLAST levels in SCA7-KI mice. We then examined HGF regulation of GLT-1, another glutamate transporter that is also abundant in the cerebellum, by a similar mechanism. Immunostaining for GLT-1 revealed that the levels of GLT-1 were markedly decreased in SCA7-KI mice compared to WT mice, while the level was maintained or even increased in SCA7-KI/HGF-Tg mice (Fig. 4D and E). These findings demonstrate that HGF maintains or even increases the levels of GLT-1 in SCA7-KI mice.

3.7. Overexpression of HGF improves rotarod performance in SCA7-KI mice

Data obtained so far suggested that SCA7 could be improved by HGF *via* the attenuation of Purkinje cellular degeneration and reduction of glutamate transporters in Bergmann glia. Therefore, we examined whether these improvements were reflected by

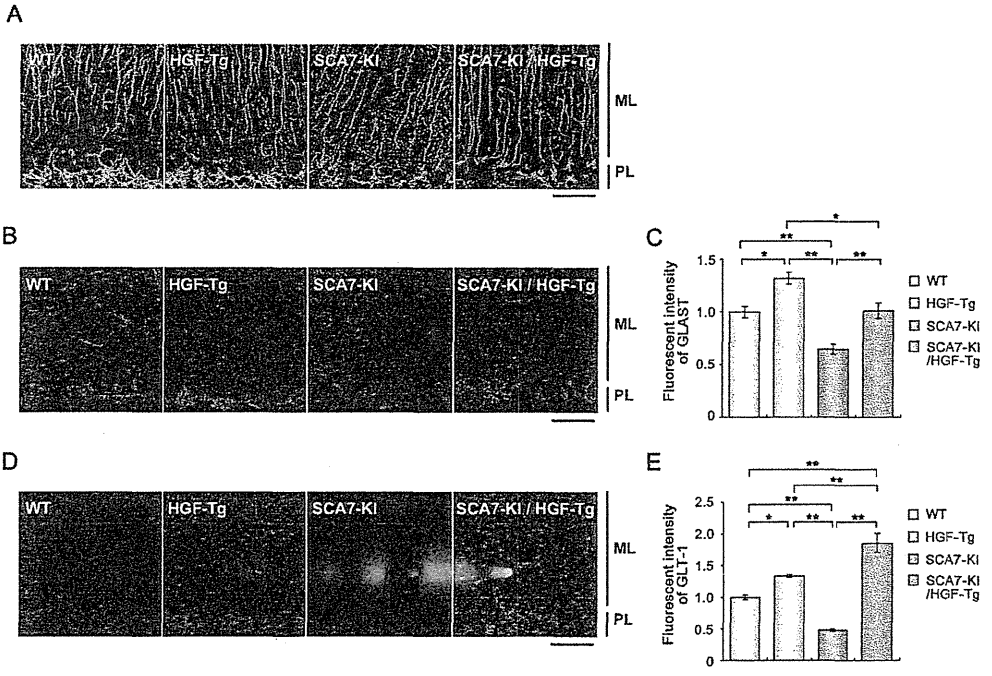

Fig. 4. HGF maintains the levels of glutamate transporters (GLAST and GLT-1) in Bergmann glia in the cerebellum of SCA7-KI mice. (A) Immunohistochemistry for Bergmann glia (GFAP, green) in the cerebellum in 10-week-old mice. No significant alterations were detected in the morphology of Bergmann glia. PL, Purkinje cell layer; ML, molecular layer. Bar, 30 μm. (B and C) Comparison of GLAST levels in 10-week-old mice. (B) Immunohistochemistry for GLAST in the cerebellum. GLAST staining is reduced in the SCA7-KI mouse cerebellum and is significantly rescued in the SCA7-KI/HGF-Tg cerebellum. Bar, 30 μm. (C) Quantification of fluorescent intensity ($n = 3$ per group) of PL. Mean GLAST signal intensity is significantly elevated in SCA7-KI/HGF-Tg cerebellum *versus* SCA7-KI cerebellum (*$P < 0.05$, **$P < 0.01$, Fisher's PLSD test). Error bars indicate S.E.M. (D and E) Comparison of GLT-1 level at 10-week-old mice. (D) Immunohistochemistry for GLT-1 in the cerebellum. GLT-1 staining is reduced in the cerebellum of SCA7-KI mice, while significantly elevated in the cerebellum of SCA7-KI/HGF-Tg mice. Bar, 30 μm. (E) Mean fluorescent intensity ($n = 3$ per group) of PL. Mean GLT-1 signal intensity is significantly elevated in the cerebellum of SCA7-KI/HGF-Tg mice (*$P < 0.05$, **$P < 0.01$, Fisher's PLSD test). Error bars indicate S.E.M. (For interpretation of the references to color in this figure caption, the reader is referred to the web version of the article.)

Please cite this article in press as: Noma, S., et al., Overexpression of HGF attenuates the degeneration of Purkinje cells and Bergmann glia in a knockin mouse model of spinocerebellar ataxia type 7. Neurosci. Res. (2012), doi:10.1016/j.neures.2012.03.001

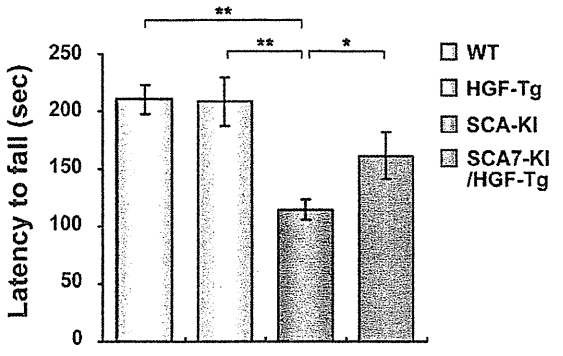

Fig. 5. HGF improves coordinated motor behavior of SCA7-KI mice. Comparison of motor coordination in 10-week-old WT, HGF-Tg, SCA7-KI, and SCA7-KI/HGF-Tg mice using the rotarod test. SCA7-KI/HGF-Tg mice display improved rotarod performance compared to SCA7-KI mice ($n = 8–12$ per group; $^*P < 0.05$, $^{**}P < 0.01$, Student's t test). Error bars indicate S.E.M.

motor performance of WT, HGF-Tg, SCA7-KI, and SCA7-KI/HGF-Tg mice. To examine the ability of an animal to balance on a rotating rod, rotarod tests were applied on each animal at 10 weeks of age. There was a marked reduction in the latency to fall in SCA7-KI mice compared to WT and HGF-Tg mice. However, the latency to fall of SCA7-KI/HGF-Tg mice was significantly longer than that of SCA7-KI mice (Fig. 5), suggesting that overexpression of HGF contributes to the amelioration of rotarod performance impairments in SCA7-KI mice.

4. Discussion

In the present study, we examined whether overexpression of HGF, a pleiotrophic growth factor with highly potent neurotrophic activities, exhibits a beneficial function in SCA7-KI mice. By crossing SCA7-KI mice with HGF-Tg mice that overexpress HGF under the NSE promoter, four groups of mice (WT, HGF-Tg, SCA7-KI, and SCA7-KI/HGF-Tg mice) were generated. The results indicate that overexpression of HGF attenuates the degeneration of Purkinje cells, maintains the levels of the glutamate transporters GLAST and GLT-1 in Bergmann glia and improves rotarod performance deficits observed in SCA7-KI mice.

The molecular mechanisms responsible for these events have not yet been clarified in detail. However, because HGF protein is expressed and distributed in Purkinje cells and Bergmann glia in SCA7-KI/HGF-Tg mice at much higher levels than in SCA7-KI mice, and because the expression and phosphorylation (activation) of c-Met was observed at much higher levels in both the Purkinje cells and Bergmann glia of SCA7-KI/HGF-Tg mice, it seems likely that HGF functions directly on Purkinje cells as well as Bergmann glia. If there is a direct interaction, the ability of HGF to function not only on Purkinje cells but also on Bergmann glia might represent a therapeutic opportunity for attenuating the degeneration of Purkinje cells, since recent genetic approaches suggest that an important mutual interaction of Purkinje cells and Bergmann glia in SCA7 might, at least in part, be involved in the degeneration of these cells in this disease (Custer et al., 2006; Furrer et al., 2011). Furthermore, Bergmann glia are also shown to secrete neurotrophic factors that support Purkinje cells (Mount et al., 1995).

Purkinje cells are integrated into a complex neural network and receive glutamatergic input from axons projecting from the inferior olive and cerebellar granule cells. Hence, in addition to Purkinje cells and Bergmann glia, which we focused on the present study, other cells and their neural networks in the cerebellum may also play a role in the pathogenesis of disease models of SCA7 and related diseases (Gatchel et al., 2007; Furrer et al., 2011). For example, transcriptional down-regulation of insulin-like growth factor binding protein 5 (*igfbp5*) in cerebellar granule cells is proposed to be involved in non-cell-autonomous degeneration of Purkinje cells in SCA7-KI mice (Gatchel et al., 2007). It has not yet been determined whether HGF could alleviate reduction of *igfbp5*, and this possibility is worth examining in a future study. Given that HGF elicits neurotrophic activity on cerebellar granular cells both *in vitro* and *in vivo* (Zhang et al., 2000; Ieraci et al., 2002), we cannot exclude the possibility that HGF functions on granular cells and alleviates the down-regulation of *igfbp5*. Therefore, HGF may also contribute to attenuation of Purkinje cell degeneration *via* cerebellar granular cells.

It has not yet been determined whether HGF alleviates the degeneration of the retina, the other region associated with phenotypic changes appearing in SCA7-KI mice. HGF and c-Met are expressed in various populations of rat retinal neurons during development as well as in the adult, and neuroprotective effects of HGF on rat retinal photoreceptors have been reported (Machida et al., 2004; Ohtaka et al., 2006; Shibuki et al., 2002; Sun et al., 1999).

The rotarod test is used to analyze motor phenotype, in the aspect of motor balance and/or its coordination (Carter et al., 2001; Custer et al., 2006). Hence, the ability of HGF to improve rotarod performance raises the potential utility of HGF for the improvement of motor impairment of affected individuals. However, further experiments are required to address the relationship between the outcome of rotarod tests in the present study and the clinical ataxic phenotype of SCA7.

Cvetanovic et al. (2011) recently reported that genetic overexpression or pharmacologic infusion of recombinant vascular endothelial growth factor (VEGF) ameliorates the ataxic phenotype and degeneration of Purkinje cells in a mouse model of another type of spinocerebellar ataxia, spinocerebellar ataxia type 1 (SCA1). Given that HGF promotes angiogenesis in a variety of disease models (Funakoshi and Nakamura, 2003, 2011) and that c-Met is not only expressed in Purkinje cells and Bergmann glia but also in other types of cells including vascular cells and neural progenitor populations in WT mice (Funakoshi and Nakamura, 2011; Noma et al., unpublished results), it would be interesting to know how HGF plays a role in SCA1-model mice and whether HGF promotes angiogenesis and neurogenesis in SCA7-KI mice. It should be noted that exercise produces beneficial effects in alleviating SCA1 symptoms in mice (Fryer et al., 2011). Exercise is known to promote HGF production in some patients (Yasuda et al., 2004) and that HGF improves the phenotype of SCA7-KI as shown in the present study. Hence, it would also be interesting to examine whether exercise plays a role in the attenuation of the progression of the course of SCA7-KI pathology and if HGF is involved in the process.

In summary, the present study provided the first evidence that overexpression of HGF is beneficial for attenuating the degeneration of both Purkinje cells and Bergmann glia. Considered with the notion that intrathecal injection of recombinant human HGF protein has been shown to be effective in several disease models, such as a transgenic rat model of ALS (Ishigaki et al., 2007) and a primate model of spinal cord injury (Kitamura et al., 2011), our findings may raise the possibility of a therapeutic use of HGF in SCA7 and related disorders.

Acknowledgements

This work was supported in part by Grants-in-Aid from the Ministry of Health, Labour and Welfare of Japan and Grants-in-Aid from the Ministry of Education, Science, and Culture of Japan. We wish to thank Prof. Huda Y. Zoghbi for providing us the SCA7-KI mice. We are grateful to Ms. Higano, Ms. Ikushima and Ms. Yoneda for secretarial assistance.

Please cite this article in press as: Noma, S., et al., Overexpression of HGF attenuates the degeneration of Purkinje cells and Bergmann glia in a knockin mouse model of spinocerebellar ataxia type 7. Neurosci. Res. (2012), doi:10.1016/j.neures.2012.03.001

References

Carter, R.J., Morton, J., Dunnett, S.B., 2001. Motor coordination and balance in rodents. Curr. Protoc. Neurosci. (Chapter 8): Unit 8.12.

Custer, S.K., Garden, G.A., Gill, N., Rueb, U., Libby, R.T., Schultz, C., Guyenet, S.J., Deller, T., Westrum, L.E., Sopher, B.L., La Spada, A.R., 2006. Bergmann glia expression of polyglutamine-expanded ataxin-7 produces neurodegeneration by impairing glutamate transport. Nat. Neurosci. 9, 1302–1311.

Cvetanovic, M., Patel, J.M., Marti, H.H., Kini, A.R., Opal, P., 2011. Vascular endothelial growth factor ameliorates the ataxic phenotype in a mouse model of spinocerebellar ataxia type 1. Nat. Med. 17, 1445–1447.

Fryer, J.D., Yu, P., Kang, H., Mandel-Brehm, C., Carter, A.N., Crespo-Barreto, J., Gao, Y., Flora, A., Shaw, C., Orr, H.T., Zoghbi, H.Y., 2011. Exercise and genetic rescue of SCA1 via the transcriptional repressor Capicua. Science 334, 690–693.

Funakoshi, H., Nakamura, T., 2003. Hepatocyte growth factor: from diagnosis to clinical applications. Clin. Chim. Acta 327, 1–23.

Funakoshi, H., Nakamura, T., 2011. Hepatocyte growth factor (HGF): neurotrophic functions and therapeutic implications for neuronal injury/diseases. Curr. Signal Transduct. Ther. 6, 156–167.

Furrer, S.A., Mohanachandran, M.S., Waldherr, S.M., Chang, C., Damian, V.A., Sopher, B.L., Garden, G.A., La Spada, A.R., 2011. Spinocerebellar ataxia type 7 cerebellar disease requires the coordinated action of mutant ataxin-7 in neurons and glia, and displays non-cell-autonomous Bergmann glia degeneration. J. Neurosci. 31, 16269–16278.

Huang, H., Bordey, A., 2004. Glial glutamate transporters limit spillover activation of presynaptic NMDA receptors and influence synaptic inhibition of Purkinje neurons. J. Neurosci. 24, 5659–5669.

Honda, S., Kagoshima, M., Wanaka, A., Tohyama, M., Matsumoto, K., Nakamura, T., 1995. Localization and functional coupling of HGF and c-Met/HGF receptor in rat brain: implication as neurotrophic factor. Brain Res. Mol. Brain Res. 32, 197–210.

Hossain, M.A., Russell, J.C., Gomez, R., Laterra, J., 2002. Neuroprotection by scatter factor/hepatocyte growth factor and FGF-1 in cerebellar granule neurons is phosphatidylinositol 3-kinase/akt-dependent and MAPK/CREB-independent. J. Neurochem. 81, 365–378.

Ieraci, A., Forni, P.E., Ponzetto, C., 2002. Viable hypomorphic signaling mutant of the Met receptor reveals a role for hepatocyte growth factor in postnatal cerebellar development. Proc. Natl. Acad. Sci. U.S.A. 99, 15200–15205.

Ishigaki, A., Aoki, M., Nagai, M., Warita, H., Kato, S., Kato, M., Nakamura, T., Funakoshi, H., Itoyama, Y., 2007. Intrathecal delivery of hepatocyte growth factor from amyotrophic lateral sclerosis onset suppresses disease progression in rat amyotrophic lateral sclerosis model. J. Neuropathol. Exp. Neurol. 66, 1037–1044.

Kadoyama, K., Funakoshi, H., Ohya, W., Nakamura, T., 2007. Hepatocyte growth factor (HGF) attenuates gliosis and motoneuronal degeneration in the brainstem motor nuclei of a transgenic mouse model of ALS. Neurosci. Res. 59, 446–456.

Kitamura, K., Fujiyoshi, K., Yamane, J., Toyota, F., Hikishima, K., Nomura, T., Funakoshi, H., Nakamura, T., Aoki, M., Toyama, Y., Okano, H., Nakamura, M., 2011. Human hepatocyte growth factor promotes functional recovery in primates after spinal cord injury. PLoS One 6, e27706.

Machida, S., Tanaka, M., Ishii, T., Ohtaka, K., Takahashi, T., Tazawa, Y., 2004. Neuroprotective effect of hepatocyte growth factor against photoreceptor degeneration in rats. Invest. Ophthalmol. Vis. Sci. 45, 4174–4182.

Miyazawa, T., Matsumoto, K., Ohmichi, H., Katoh, H., Yamashima, T., Nakamura, T., 1998. Protection of hippocampal neurons from ischemia-induced delayed neuronal death by hepatocyte growth factor: a novel neurotrophic factor. J. Cereb. Blood Flow Metab. 18, 345–348.

Mount, H.T., Dean, D.O., Alberch, J., Dreyfus, C.F., Black, I.B., 1995. Glial cell line-derived neurotrophic factor promotes the survival and morphologic differentiation of Purkinje cells. Proc. Natl. Acad. Sci. U.S.A. 92, 9092–9096.

Nakamura, T., Nawa, K., Ichihara, A., 1984. Partial purification and characterization of hepatocyte growth factor from serum of hepatectomized rats. Biochem. Biophys. Res. Commun. 122, 1450–1459.

Nakamura, T., Nishizawa, T., Hagiya, M., Seki, T., Shimonishi, M., Sugimura, A., Tashiro, K., Shimizu, S., 1989. Molecular cloning and expression of human hepatocyte growth factor. Nature 342, 440–443.

Ohtaka, K., Machida, S., Ohzeki, T., Tanaka, M., Kurosaka, D., Masuda, T., Ishii, T., 2006. Protective effect of hepatocyte growth factor against degeneration of the retinal pigment epithelium and photoreceptor in sodium iodate-injected rats. Curr. Eye Res. 31, 347–355.

Ohya, W., Funakoshi, H., Kurosawa, T., Nakamura, T., 2007. Hepatocyte growth factor (HGF) promotes oligodendrocyte progenitor cell proliferation and inhibits its differentiation during postnatal development in the rat. Brain Res. 1147, 51–65.

Shibuki, H., Katai, N., Kuroiwa, S., Kurokawa, T., Arai, J., Matsumoto, K., Nakamura, T., Yoshimura, N., 2002. Expression and neuroprotective effect of hepatocyte growth factor in retinal ischemia-reperfusion injury. Invest. Ophthalmol. Vis. Sci. 43, 528–536.

Sun, W., Funakoshi, H., Nakamura, T., 1999. Differential expression of hepatocyte growth factor and its receptor, c-Met in the rat retina during development. Brain Res. 851, 46–53.

Sun, W., Funakoshi, H., Nakamura, T., 2002. Overexpression of HGF retards disease progression and prolongs life span in a transgenic mouse model of ALS. J. Neurosci. 22, 6537–6548.

Yamada, A., Matsumoto, K., Iwanari, H., Sekiguchi, K., Kawata, S., Matsuzawa, Y., Nakamura, T., 1995. Rapid and sensitive enzyme-linked immunosorbent assay for measurement of HGF in rat and human tissues. Biomed. Res. 16, 105–114.

Yasuda, S., Goto, Y., Takaki, H., Asaumi, Y., Baba, T., Miyazaki, S., Nonogi, H., 2004. Exercise-induced hepatocyte growth factor production in patients after acute myocardial infarction: its relationship to exercise capacity and brain natriuretic peptide levels. Circ. J. 68, 304–307.

Yoo, S.Y., Pennesi, M.E., Weeber, E.J., Xu, B., Atkinson, R., Chen, S., Armstrong, D.L., Wu, S.M., Sweatt, J.D., Zoghbi, H.Y., 2003. SCA7 knockin mice model human SCA7 and reveal gradual accumulation of mutant ataxin-7 in neurons and abnormalities in short-term plasticity. Neuron 37, 383–401.

Zhang, L., Himi, T., Morita, I., Murota, S., 2000. Hepatocyte growth factor protects cultured rat cerebellar granule neurons from apoptosis via the phosphatidylinositol-3 kinase/Akt pathway. J. Neurosci. Res. 59, 489–496.

Please cite this article in press as: Noma, S., et al., Overexpression of HGF attenuates the degeneration of Purkinje cells and Bergmann glia in a knockin mouse model of spinocerebellar ataxia type 7. Neurosci. Res. (2012), doi:10.1016/j.neures.2012.03.001

SAGE-Hindawi Access to Research
Leukemia Research and Treatment
Volume 2011, Article ID 726964, 11 pages
doi:10.4061/2011/726964

Review Article

Characterization of Kaposi's Sarcoma-Associated Herpesvirus-Related Lymphomas by DNA Microarray Analysis

Keiji Ueda, Eriko Ohsaki, Kazushi Nakano, and Xin Zheng

Division of Virology, Department of Microbiology and Immunology, Osaka University Graduate School of Medicine, 2-2 Yamada-oka, Suita, Osaka 565-0871, Japan

Correspondence should be addressed to Keiji Ueda, kueda@virus.med.osaka-u.ac.jp

Received 26 June 2011; Accepted 2 September 2011

Academic Editor: Daniela Cilloni

Among herpesviruses, γ-herpesviruses are supposed to have typical oncogenic activities. Two human γ-herpesviruses, Epstein-Barr virus (EBV) and Kaposi's sarcoma-associated herpesvirus (KSHV), are putative etiologic agents for Burkitt lymphoma, nasopharyngeal carcinoma, and some cases of gastric cancers, and Kaposi's sarcoma, multicentric Castleman's disease, and primary effusion lymphoma (PEL) especially in AIDS setting for the latter case, respectively. Since such two viruses mentioned above are highly species specific, it has been quite difficult to prove their oncogenic activities in animal models. Nevertheless, the viral oncogenesis is epidemiologically and/or *in vitro* experimentally evident. This time, we investigated gene expression profiles of KSHV-oriented lymphoma cell lines, EBV-oriented lymphoma cell lines, and T-cell leukemia cell lines. Both KSHV and EBV cause a B-cell-originated lymphoma, but the gene expression profiles were typically classified. Furthermore, KSHV could govern gene expression profiles, although PELs are usually coinfected with KSHV and EBV.

1. Introduction

Several viruses could induce cancers in human beings. For examples, some papilloma viruses (PVs) should be etiologic agents for cervical cancers [1], hepatitis B virus (HBV) [2] and hepatitis C virus (HCV) [3] for hepatocellular carcinomas, human T-lymphotropic virus 1 (HTLV-1) for adult T-cell leukemia (ATL) [4], Epstein-Barr virus (EBV) for Burkitt lymphomas, nasopharyngeal carcinomas (NPCs), and some of gastric carcinomas [5, 6], and Kaposi's sarcoma-associated virus (KSHV) for Kaposi's sarcoma [7], primary effusion lymphomas (PELs), and multicentric Castleman's disease [8–13]. Recently, a newly identified polyomavirus, Merkel cell polyomavirus, is nominated as an etiologic agent for Merkel cell carcinoma [14]. These viruses have too narrow host ranges to meet Koch's principles, and, therefore, there are a lot of augments about it. Nevertheless, causation between the viral infection and the related cancer formation could be evident epidemiologically and *in vitro* experimentally.

Chronic inflammation caused by these viruses should be important factors, but it is not forgettable to keep in our minds that such inflammation itself is primarily caused by the viral infection [17]. Except for HCV and HTLV-1, these oncogenic viruses are usually DNA viruses and establish persistent or latent infection [18, 19]. Of course, HCV also establishes persistent infection in the infected hepatocytes [3]. Parts of some viral genomes in case of DNA viruses are integrated into host genomes, even though the process is not included in the life cycles. Integration could play roles for oncogenesis as shown for retroviral oncogenesis, and; thus, integration of viral genomes leads to promoter insertion mechanism to activate putative cellular oncogenes and host genome fragility [20]. If viral oncogenes are integrated and expressed, the effect should be more direct.

γ-herpesviruses such as EBV and KSHV are DNA viruses and do not have the genome integration process in their life cycles and just present as episomes in the infected nuclei for lives after establishing latent infection, since their genomes replicate and are partitioned according to the host cell cycles by utilizing host cellular replication machinery [6, 9]. Thus, the genomes act as complete extra genomes.

KSHV was found in Kaposi's sarcoma tissues with representational difference analysis (RDA) as the eighth human herpesvirus by Chang et al. [21]. The sequence analysis revealed that this virus is not a member of $\gamma 1$ or lymphocryptoviruses, which includes EBV, but $\gamma 2$ or rhadinoviruses, whose prototype is Herpesvirus saimiri [22]. Extensive studies about the relationship between the virus infection and the diseases have shown that this virus is a causative agent for Kaposi's sarcoma [7], primary effusion lymphomas (PELs), and multicentric Castleman's disease [8], most of which happen in acquired immunodeficiency syndrome setting [23]. As for KS, KSHV is usually present in all types of KS: classical, iatrogenic, and African endemic KS and human immunodeficiency virus-1 negative gay men with KS [24]. Thus, it is doubtless that KSHV is an etiologic agent for KS and two lymphoproliferative diseases such as PEL and MCD as various kinds of γ-herpesviruses are related to some cancer formation [19].

KSHV has two life cycles: lytic infection/reactivation and latent infection as known for all herpesviruses. Among eight human herpesviruses, only EBV and KSHV establish latency *in vitro* especially Burkitt lymphoma [25] cell lines and PEL cell lines, respectively. In the latency, the viruses express a limited number of genes and replicate according to host cell cycle. The replicated genomes are partitioned into daughter cells, and; thus, the same copy number of the viral episomes is maintained, though details of the mechanism remain to be elucidated [26].

In case of KSHV, the viral latency seems to be very important for the maintenance of PEL, since the loss of the viral episomes leads to PEL cell death. Furthermore, EBV and KSHV usually coinfected in PEL but EBV is frequently lost while establishing PEL cell lines [27]. It has been unable for us to find out or establish subclones of KSHV-negative PEL cell lines from the parental lines [28]. In contrast, an EBV-lost BL cell line has been established [29].

Recently, we investigated gene expression profiles of several PEL cell lines [30] TY1 [31], BCBL1 [32], and its derivative D90 [28], BC3 [27], BC1 [33], in order to know the characteristic gene expression to maintain the PEL cells, comparing with those of BL lines: Ramos, Daudi, BJAB, Raji, and Akata [34]. And including T-cell-originated lymphoma cell lines: Jurkat, Molt3, SupT1 and MT4, we tried to know common features leading to lymphoma formation. Among PEL cell lines, only BC1 is coinfected with KSHV and EBV. BL cell lines are usually infected with EBV except Ramos and BJAB in the lineups this time. MT4 contains integrated human T-cell leukemia virus 1 (HTLV-1) genomes. Typically, the gene expression profiles were classified into either B-cell-originated or T-cell-originated pattern. And KSHV-associated PEL and usually EBV-associated BL showed typical gene expression profiles, respectively. Even though there was only one PEL cell line infected both with KSHV and EBV, its gene expression profile was classified as a KSHV pattern, suggesting that KSHV might make stronger influence on gene expression in the infected cells. In this paper, we would like to discuss and review about gene expression profiles of KSHV-associated B-cell lymphoma or lymphoma-like disease, while mining new data from our DNA array analysis or comparing ours to the others.

2. Gene Expression Profiles of KSHV-Related Tumors

As mentioned above, there are three definite diseases caused by KSHV. They are KS, PEL, and MCD. Especially in AIDS setting, KSHV has a very tight link with these diseases, and that is the virulence of KSHV emerges under the condition. It seems to be meaningful to know gene expression profiles of tumors, since such gives us information about origin of tumor cells, mechanism of tumorigenesis, designs of treatment, and so on. And thus; several reports have been published [25].

2.1. Kaposi's Sarcoma. The cellular origin of the spindle cells of KS is poorly defined and could be originated from vascular endothelial cells and various kinds of cytokines, chemokines, and growth factors are expressed [35, 36]. A recent report has shown that KSHV reprograms transcription profiles from angiogenic to lymphatic ones by inducing *PROX1*, a master regulator of lymphatic development and downregulation of blood vascular genes, in infected human dermal microvascular endothelial cells (HDMECs) [37, 38]. KSHV induces LYVE-1, reelin, follistatin, and desmoplakin as well as *PROX1*. These findings suggest that KSHV infection should induce a comprehensive reprogramming of blood vascular endothelial cells (BECs) to adopt a lymphatic endothelial cells (LECs). In the tissues of KS, a kind of cytokine and interleukin-6 (IL-6), basic fibroblast growth factor (bFGF), tumor necrosis factor-α (TNF-α), oncostatin M, interferon-γ (IFN-γ), and so on storm happens. In *in vitro* KSHV infection study; however, IL-6, oncostatin M, TNF-α, and IFN-γ inductions were not induced. In contrast, tumor growth factor $\beta 1/\beta 3$ and TGFb R2, CCL5 [39], CCL8 (MCP-2) and CCR5, and angiopoietin-2 (ang-2) were induced. Though such differences might be dependent on differences from environment for preparation of samples, some factors could be synthesized and secreted from the other kinds of cell type, because KS is actually a mixture of various kinds of tissues [35]. KS is basically latently infected with KSHV, and, thus usually does not express KSHV lytic genes [40]. It is, however, possible that lytic cycle is turned on especially just upon the infection and some lytic genes such as viral IL-6 (vIL-6), viral chemokines (vMIP-I, vMIP-II, and vMIP-III), possible oncogenic genes, such as K1, viral G-protein-coupled receptor (vGPCR) are expressed transiently and make an effect on various kinds of cellular gene expression [37]. Though details about mechanism remain to be understood, replication and transcription activator (RTA), a viral immediate early gene and a key inducer of viral lytic replication, must be expressed for lytic replication cycle. RTA is an extremely strong transactivator and functions both in a sequence-specific and a nonspecific manner. RTA could induce critical cellular gene expression and make a direction to KS formation [41, 42].

2.2. Multicentric Castleman's Disease. KSHV causes two B-cell-originated lymphoproliferative diseases: MCD and PEL [16]. MCD is a polyclonal and a kind of reactive lymphoproliferative disorder characterized by KSHV-infected monotypic cytoplasmic IgM-λ-expressing plasmablasts residing primarily in the mantle zone, dissolution of the follicles, and prominent interfollicular vascular proliferation [7]. MCD cells resemble mature B cells, as they express the preplasma cell markers, IRF4 and BLIMP1, the memory B-cell marker CD27, OCT2, and Ki67, though they are negative for certain B-cell-associated marker such as Pax5, CD20, CD30, and CD138 (syndecan-1) [43]. MCD plasmablasts are reported not to show somatic hypermutation in their rearranged IgV genes [7]. KSHV might preferentially target IgM-λ-expressing native B cells and differentiate into plasmablasts bypassing the GC reaction, although not all MCDs are infected with KSHV. In MCD, EBV is rarely coinfected [44]. It seems quite an interesting story, since both of viruses can infect a B-cell lineage and EBV usually disseminates more than 90% human beings and probably preexist in B cells before KSHV enters. It is unclear and should be elucidated whether MCD does not emerge in the presence of EBV, or development of MCD excludes EBV from the cells.

It has not been successful to observe lymphoproliferation *in vitro* by infecting KSHV with peripheral blood mononuclear cells as shown for EBV, though KSHV infects $CD19^+$B cells and establishes latency therein [32, 45]. From a point of view of gene expression profiles, high level interleukin 6 (IL-6) expression is a well-known fact in MCD and should do something in MCD pathogenesis [46]. B-cell markers, CD20 and the memory B-cell marker CD27 are usually expressed, but B-cell activation markers such as CD23, CD38 and CD30 are not [43]. KSHV gene expression profiles are different from those in KS and PEL. It was reported that viral lytic genes, vIRF-1 and vIL-6, and ORF59 (a polymerase processivity factor, PF8) as well as a latent gene, LANA, were expressed, suggesting that not a few cells in MCD are in the lytic phase [47].

2.3. Primary Effusion Lymphoma (PEL). PEL is a distinct subtype of non-Hodgkin's lymphoma associated with KSHV as mentioned. PEL most commonly presents with pleural, peritoneal, or pericardial malignant effusions without a contiguous tumor mass [16]. In contrast to MCD, PEL is usually coinfected with EBV in vivo, and; therefore, EBV could be involved in the onset of tumor formation. It could be likely that PEL with or without EBV is different from origin of B-cell differentiation state [48]. KSHV, however, is never lost when PEL is introduced into cell culture maintenance *in vitro*, even if EBV frequently is lost from PEL cell lines. Thus, there is a strong linkage between the existence of KSHV and the maintenance of PEL cell lines *in vitro*. PEL is thought to be originated from post-GC plasmablastic cells [49]. Both PEL and MCD have a plasmablastic phenotype but should be different in the terms whether they are post-GC or bypass-GC reaction, respectively, [50].

EBV is another human oncogenic γ-herpesvirus, a putative causative agent of BL, NPC, some gastric carcinoma, NK lymphoma, and so on [6]. BL is also originated from GC B-cell and known for *MYC-IgH* or *MYC-IgL* rearrangement [15, 51]. Study on gene expression profiles using *in vitro* infection systems showed that cyclin-dependent kinase inhibitor 1 (CDKN1A; CIP1/WAF1; p21, U09579), interleukin-15 receptor α subunit precursor (U31628), interferon-induced 56-kd protein (IFI-56 K, X31628), and protein-tyrosine phosphatase 1C (PTP1C) SHP1 (X62055) and HLA class II histocompatibility antigen α chain (K01171) and HLA-DR antigen-associated invariant subunit (X00497) were prominently induced by the factor of ten or more [52]. High-mobility group protein (HMG-I, M23619), proliferating cyclic nuclear antigen (PCNA, M15796), endonuclease III homolog I (U79718), poly(ADP-ribose) polymerase (PARP; PPOL, M18112), erythroblastosis virus oncogene homolog1 (ETS-1, J04101), p-GAP hematopoietic protein C1 (RGC1, X78817), and c-myc (V00568) were remarkably reduced by the factor of five to eight hundred [52]. In this paper, EBV was infected with EBV-negative BL cell lines. The infected cells showed latency III phenotype, which is corresponding to lymphoblastoid cell lines (LCLs) established by EBV infection to PBMC *in vitro*. Most of BL, however, show latency I phenotype, and thus; this experiment model reflects LCL rather than BL [6]. Another report also utilized an EBV-depleted BL cell line, EBV^- Akata [53]. EBV^- Akata and EBV^+ Akata were stimulated with IgG crosslinking, and lytic replication was induced. They analyzed cellular gene expression as well as viral gene expression. In this case, data did not reflect effects of EBV on BL, since this was just lytic replication/reactivation process, and almost all viral genes were expressed, which presumably took a substantial effect on cellular gene expression.

We recently investigated gene expression profiles of PEL cell lines, comparing with those of the other uniquely categorized cell lines, one of which was BL cell lines with or without EBV infection and another of which was T-cell leukemia cell lines (TCLs) [30]. All PEL cell lines are infected with KSHV, and one of them, BC1, is coinfected with KSHV and EBV. BL cell lines are usually infected with EBV, but Ramos and BJAB are not infected with EBV. TCL cell lines are heterogeneous. Jurkat was established from an acute T-cell leukemia, and Molt-3 and SupT1 were from a respective T-lymphoblastic leukemia, and MT4 was from an adult T-cell leukemia. Thus, differentiation status may be different among lines.

Our obtained results were that three kinds of lines were typically classified into respective groups. Although the results might reflect just differentiation status of these cell lines, KSHV would never be lost from the PEL cell lines and BC1 coinfected with KSHV, and EBV was classified into the PEL cell category, suggesting that KSHV should be more dominant in gene expression control. Among about thirty thousand genes analyzed this time, we could extract sixty-three genes typically higher in BL cell lines and also sixty genes predominantly higher in PEL cell lines. For example, CD79A (NM_001738) and B (NM_000626), which are components of B-cell receptor and contain cytoplasmic immunoreceptor tyrosine-based

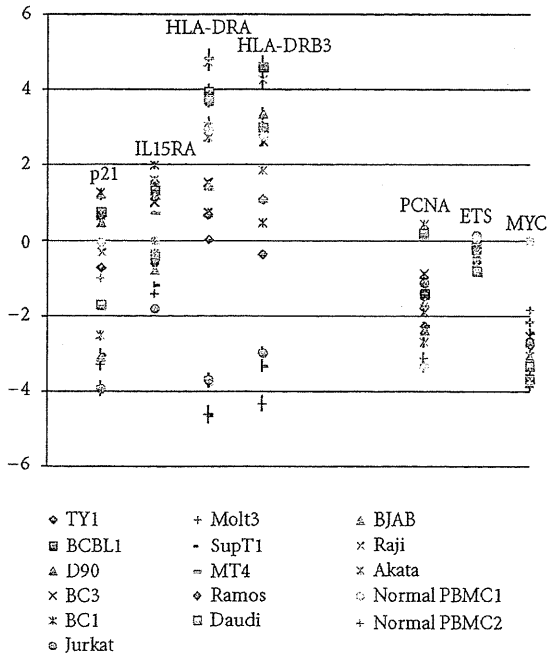

FIGURE 1: Genes increased or decreased in the presence of EBV [15] are picked up. The increased genes; $p21^{Cip1/WAF1}$, IL15RA, HLA-DRA, and HLA-DRB3 were checked. The decreased genes: PCNA, ETS, and MYC (represented as N-myc in our case) were checked. Data are shown as $\log_2$ values with standard deviation. The concrete mean value of each gene expression was shown in Table 1.

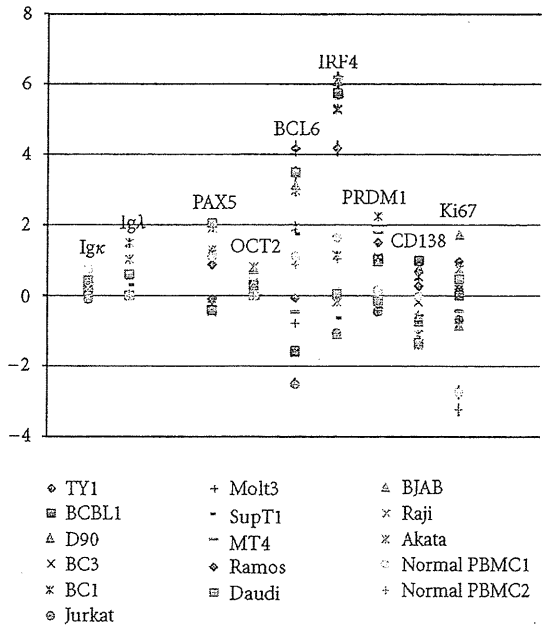

FIGURE 2: Genes characteristic in MCD are picked up. In MCD, Igκ, PAX5, BCL6, CD138 are usually not expressed [16]. On the other hand, Igλ, OCT2, IFR4/MUM1, PRDM1/BLINP1, and Ki67 are expressed [16]. Data are shown as $\log_2$ values with standard deviation. Characterization among PEL, BL, and TCL is shown in Table 2.

TABLE 1

Name	ID	TY1	BCBL1	D90	BC3	BC1	Jurkat	Molt3	SupT1	MT4	Ramos	Daudi	BJAB	Raji	Akata	Normal PBMC1	Normal PBMC2
p21, Cip1 (CDKN1A), transcript variant 1	NM-000389	0.6168	0.7342	0.4951	0.6498	1.2574	−3.9304	−3.2876	−3.0266	1.1385	−0.7121	−1.6921	−3.071	−0.2815	−2.5181	−0.0306	−0.9993
IL15RA transcript variant 1	NM-002189	1.5549	1.3211	1.2054	1.0005	1.9795	−1.7987	−1.4156	−1.1644	0.7295	−0.6013	−0.4221	−0.7741	1.5869	−0.3408	0	0
HLA-DRA	NM-019111	0.6808	3.9458	3.0478	1.5288	0.7271	−3.696	−4.6163	−4.6238	4.8328	0.0282	3.7191	1.4575	4.7263	2.7318	2.9285	3.1007
HLA-DRB3	AF192259	1.1026	4.5938	3.344	2.6277	0.4602	−2.9625	−4.33	−3.3242	4.657	−0.3435	2.9802	1.1189	4.2563	1.8549	2.7688	2.9922
PCNA, transcript variant 1	NM-002592	−2.2538	−1.4012	−2.3533	−0.8696	−1.8885	−1.111	−1.0025	−2.2581	0.0462	−1.3735	0.2045	−1.6252	−2.6854	0.4512	−3.3202	−3.1112
ETS oncogenes	L16464	−0.2124	−0.2223	−0.1314	−0.6449	−0.6913	0.1483	−0.1052	0.0186	−0.0974	−0.0638	−0.8105	−0.3384	−0.3456	−0.5868	0.0757	−0.1052
MYCN	NM-005378	−2.7601	−3.6677	−3.7899	−2.5286	−2.7087	−2.7141	−3.2058	−2.4416	−2.1501	−3.3287	−3.329	−3.0585	−3.7126	−3.0375	0	−1.8303

TABLE 2

Lines	Gene						
	IRF4/MUM1	PRDM1/BLINP1	CD138	PAX5	BCL6	OCT2	Ki67
PEL	↑↑	↑	↑	↓	↓	→	→
BL	↑	→	↓	↑	↑↑	→	→
TCL	↓	↓	↓	↓	↓	→	↓

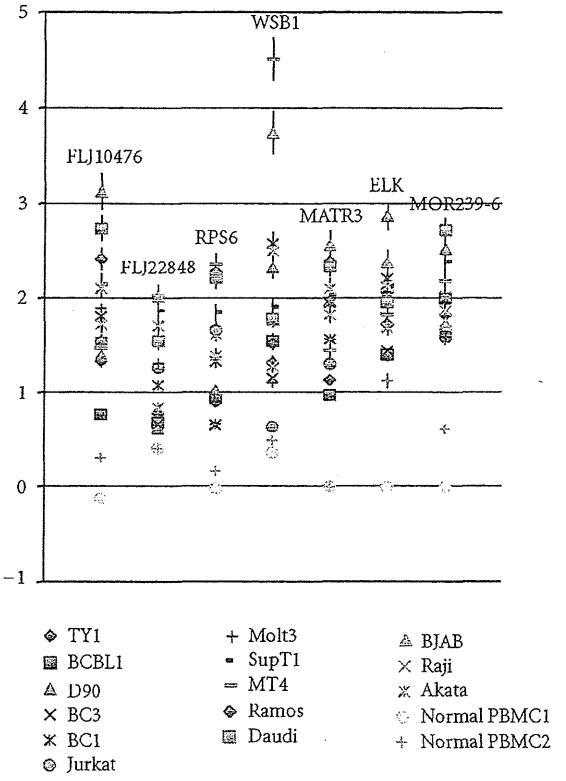

FIGURE 3: Highly expressing genes all in PEL, BL, and TCL are picked up. Data are shown as $\log_2$ values with standard deviation. Data are shown as $\log_2$ values with standard deviation. Detailed mean value of each gene is shown in Table 3.

activation motifs were highly expressed in BL without doubt. Accordingly, BCR downstream signaling 1 (BRDG1, NM_012108) was also higher in BL cell lines. A mature B cell-marker, CD22 (NM_001771), was characteristically expressed in BL not in PEL. Among very highly expressing genes in PEL, we found methyl CpG-binding domain protein (MBD1, NM_015845), interleukin 2 receptor beta (IL2RB, NM_000878), and angiopoietin 1 (ANGPT1, NM_001146). Such gene expression in PEL might suggest cellular environment and pathophysiologic status in the patient bodies under immunosuppression due to AIDS established by human immunodeficiency virus 1 (HIV-1) and KSHV infection.

Focused on $p21^{Cip1/WAF1}$ (NM_000389), IL15 receptor α (NM_002189) and HLA-DR (HLA-DRA, NM_019111; HLA-DRB3, AF192259), which are reported to increase by EBV infection, this gene expression was indeed higher in B cell originated PEL and BL with a few exceptions in our analysis (Figure 1, Table 1). PCNA, ETS (L16464), and MYC (NM_005378) were relatively higher in TCL again with several exceptions, though MYC-Ig rearrangement was a feature of BL.

Paying attention to genes characteristic to MCD, a naïve B-cell marker: surface Ig lambda (XM_066332), B-cell specific markers: PAX 5 (NM_016734), Oct2 (XM_068123), and a GC B-cell marker: BCL6 (NM_001706) were higher in BL cell lines and preplasma cell markers; IRF4/MUM1 (NM_002460) and PRDM1/BLIMP1 (NM_001198) are definitely higher in PEL cells, assuring that BL should be derived from GC B cell and PEL from post-GC plasmablasts (Figure 2, Table 2). Plasma cell marker, CD138 (NM_002997), was also higher in PEL. Memory B-cell markers, Oct2 and Ki67 (NM_002417) expression, were not so different among three types of cell lines. Collectively, decisive differences between PEL and BL are low CD138 in

TABLE 3

Name	ID	TY1	BCBL1	D90	BC3	BC1	Jurkat	Molt3	SupT1	MT4	Ramos	Daudi	BJAB	Raji	Akata	Normal PBMC1	Normal PBMC2
cDNA FLJ10476	AK001338	1.3263	0.7676	1.3801	1.7984	1.5367	1.5343	1.882	2.1362	1.4682	2.4062	2.7347	3.1228	1.7163	2.098	−0.1203	0.3065
cDNA: FLJ22848	AK026501	0.7782	0.6786	0.6153	0.6563	1.0736	1.2594	1.3044	1.8615	2.0176	1.5196	1.5458	2.0081	1.7023	0.8386	0.4045	0.4004
Ribosomal protein S6 (RPS6)	NM_001010	0.9017	0.9334	1.0244	0.6479	1.3239	1.6572	0.6572	1.8411	2.3493	2.2682	2.1999	2.2522	1.3873	1.6164	−0.0182	0.1647
WD repeat and SOCS box-containing 1 (WSB1), transcript variant 1	NM_015626	1.3127	1.5445	2.3089	1.1516	2.5711	0.6377	1.0981	1.9078	4.5103	1.5161	1.7749	3.7406	1.2755	2.4918	0.359	0.4896
Matrin 3 (MATR3)	NM_018834	1.1246	0.968	1.9522	1.5564	1.9376	1.2933	1.5574	2.0226	1.4332	2.3825	2.3212	2.5539	1.8178	2.0884	0	0
ELK (LOC131341)	XM_067332	1.7184	1.391	2.8614	1.4346	2.1936	2.0576	2.0501	2.1184	1.813	1.9541	1.9471	2.3651	2.1104	1.6868	0	1.121
Similar to olfactory receptor MOR239-6	XM_372502	1.6318	1.9947	2.5101	1.6554	2.706	1.5783	1.5849	2.3774	2.1667	1.8178	2.711	1.7203	1.8556	2.0178	0	0.603

TABLE 4

Name	ID	TY1	BCBL1	D90	BC3	BC1	Jurkat	Molt3	SupT1	MT4	Ramos	Daudi	BJAB	Raji	Akata	Normal PBMC1	Normal PBMC2
cDNA FLJ20118	AK000125	−2.3823	−1.9072	−1.9797	−1.8911	−2.6889	0	−2.1411	−3.2798	−2.5236	−2.1555	−2.0963	−2.7591	−1.9995	−3.0018	0	0
cDNA FLJ12884	AK022946	−2.8453	−2.4261	0	−2.737	−2.4877	−2.3244	−0.8999	−1.0235	−1.4208	−2.4356	−3.054	−3.0835	−2.7217	−2.5435	0	0
cDNA FLJ13038	AK023100	−2.9994	−2.4772	−3.0186	−3.3026	−2.7287	−3.3596	−0.9996	−0.183	−2.7834	−2.658	−2.4415	−2.4291	−2.2883	−2.1052	0.3132	0.1399
cDNA FLJ13209	AK023271	−2.9254	−3.6178	−3.8287	−3.3465	−2.8999	−2.3812	−4.33	−2.8324	−3.6977	−3.658	−3.481	−3.5892	−3.4616	−3.7744	0	−0.5065
cDNA FLJ14567	AK027473	−3.3823	−3.6178	−2.7058	−1.8379	−3.0182	−1.3668	−2.0374	−2.2945	−1.1757	−3.073	−2.6242	−3.8415	−3.3297	−2.4208	0	−1.7585
cDNA FLJ31353	AK055915	−3.5001	−4.7198	−4.1118	−3.7967	−3.6791	−2.7417	−3.8866	−2.9092	−4.0524	−3.0009	−2.66	−2.2996	−1.3509	−4.1115	−0.3823	−0.1246
cDNA FLJ37955	AK095274	−1.2998	−0.1113	−1.5633	−1.317	−0.7984	−2.5666	−1.8192	−1.5649	−0.9224	−1.412	−2.5134	−2.0463	−2.5324	−1.4445	0	0
Odz3	AK125869	−2.0213	−2.4624	−1.4756	−1.3957	0	−2.9199	−2.5731	0	−2.6255	−2.2639	−2.4891	−2.0586	−2.4616	−2.5606	0	−1.0642
COL1A2	NM_000089_(2)	−3.44	−3.3222	−4.0878	−4.1915	−2.749	−3.696	−3.9297	0	−3.7933	−3.1489	−3.2724	−3.3744	−3.2883	−3.7349	0	0
Cystatin C (CST3)	NM_000099	−2.4327	−4.907	−6.1118	−1.2356	−5.4965	−2.5502	−3.4042	−3.4663	−1.4284	−5.6953	−6.1657	−2.9177	−5.7681	−5.5523	0.8547	1.1031
HBG2	NM_000184	−3.0213	−3.5694	−5.6968	−4.589	−3.1337	−4.9735	−5.8868	−4.6997	−5.983	−4.989	−5.0186	−4.4372	−6.0162	−5.7744	2.1347	0.3396
LYZ	NM_000239	−5.6627	−5.492	−6.0191	−3.9692	−5.5666	−6.0181	−5.1158	−5.3856	−5.3393	−5.8556	−4.8031	−4.7591	−5.3724	−4.9903	3.8701	4.0167
Serine (or cysteine) proteinase inhibitor	NM_000295	−5.2996	−1.4884	−4.5925	−5.7768	−5.245	−5.9302	−6.0676	−5.5169	−5.8128	−5.4198	−5.973	−5.8415	−5.7681	−5.5523	−1.0957	−1.0244
Interleukin 8 (IL8)	NM_000584	−3.066	−2.2442	−1.7518	−3.2322	−2.2886	−1.9093	−1.5561	−2.3167	−1.0642	−0.786	−2.1655	−2.3976	−1.9719	−0.8359	0.2761	1.0034
Interleukin 8 (IL8)	NM_000584_(2)	−4.5312	−3.1113	−3.6435	−2.4952	−3.6218	−3.7141	−3.7453	−2.7393	−2.7447	−4.3286	−4.4183	−2.8521	−3.5085	−3.4525	0.6967	1.5545
ANXA1	NM_000700	−1.6884	−2.7462	−5.7704	−4.139	−2.1007	−5.5584	−1.2667	−0.7569	−1.2654	−5.1886	−5.8851	−5.7587	−5.6238	−5.3593	−0.1914	−0.0244
TNFRSF1B	NM_001066	−0.0646	0.4257	−0.2587	1.098	0.1654	0.2687	0.0731	0.1623	0.208	−0.3584	−0.6991	0.0238	0.6067	−0.1162	2.0232	2.1586
ANPEP	NM_001150	−2.4773	−1.7507	−2.6092	−2.7866	−2.7593	−3.0066	−3.0552	−2.458	−2.3106	−1.6907	−2.3004	−2.5452	−2.1459	−2.0679	0.5172	0.5893
APOC1	NM_001645	−3.6284	−3.538	−2.7898	−3.554	−3.8226	−3.9735	−4.6522	−3.2088	−3.1376	−3.814	−4.0902	−3.9982	−3.6943	−4.0374	0	0
CRYAB	NM_001885	−1.994	−2.3767	−2.7519	−2.8275	−1.1204	−1.4943	−2.7645	−1.347	−1.245	−1.2816	−2.2518	−1.4818	−2.3089	−1.4287	0	0
GZMK	NM_002104	−3.7509	−1.7642	−3.2504	−2.8275	−3.0557	−3.9954	−3.6702	−3.6613	−2.8032	−2.2499	−3.3004	−2.2636	−2.2547	−2.2233	0.5673	0.6936
JUN	NM_002228	−2.2409	−2.7734	−3.1238	−0.3842	−1.8718	−0.968	−0.4387	−0.1644	−0.0479	−0.1719	−4.1148	−2.9517	−2.454	−3.7744	1.5962	0.4284
CD73 (NT5E)	NM_002526	−3.5469	−3.5694	−2.9525	−2.1262	−4.3968	−2.9955	−3.0552	−3.4173	−3.0405	−4.162	−3.53	−2.5027	−3.4164	−3.0495	0	0

Table 4: Continued.

Name	ID	TY1	BCBL1	D90	BC3	BC1	Jurkat	Molt3	SupT1	MT4	Ramos	Daudi	BJAB	Raji	Akata	Normal PBMC1	Normal PBMC2
PLAU	NM_002658	−1.32	−1.3256	−1.0046	−1.9922	0	−1.7095	−2.8448	0	0	−1.564	−2.6154	−2.3216	−2.005	−2.4366	0	0
CCL4	NM_002984	−4.0775	−3.0884	−3.2772	−3.6609	−3.8663	−4.0179	−4.2461	−3.7799	−3.2966	−3.8773	−3.1025	−3.0341	−0.0679	−2.7947	−0.2159	0.5398
ADAM12	NM_003474	−3.2734	−2.4118	−2.4872	−3.9021	−3.1744	−2.7141	−2.8448	−4.1018	−1.7494	−1.4316	−2.245	−2.8415	−2.3438	−1.2267	0	0
CST7	NM_003650	−4.8452	−3.9896	−4.0644	−4.9018	−4.4624	−2.9199	−2.9627	−3.2088	−3.7163	−3.0126	−3.7061	−3.8629	−3.59	−3.1371	−0.4389	−0.3123
Transmembrane protein with EGF-like	NM_003692_(2)	−2.671	−2.4047	0	−2.7765	−2.8225	−0.806	−1.1992	−1.3585	−2.3392	−2.3888	−2.642	−2.2147	0.3012	−2.8359	0	0
SEMA5A	NM_003966	−2.8649	−1.8483	0	−2.4386	−2.8885	−2.9304	−3.0552	−2.5429	−1.7116	−0.949	−2.1785	−2.5281	−1.9556	−1.4326	0	0
GNG11	NM_004126	−4.0104	−3.4189	−4.3748	−3.2049	−4.0558	−3.696	−3.9517	−4.0512	−3.2966	−4.0608	−3.9956	−2.2285	−3.0276	−3.535	0.048	0.2964
GZMB	NM_004131	−2.8163	−2.7373	−3.1483	−2.4788	−2.5577	−2.6085	−2.9627	−3.141	−2.1376	−2.5947	−3.4031	−3.0585	−2.8869	−2.5097	−0.3744	0.161
CSPG2	NM_004385	−2.8949	−2.3492	−3.3043	−2.6702	−3.2887	−3.3739	−3.4663	−3.6804	−1.2017	−3.0009	−3.4493	−2.8846	−2.8665	−3.4849	2.5309	2.5699
DUSP1	NM_004417	−2.0379	−0.9817	−1.9471	−1.6749	−1.8718	−1.5061	−0.9489	−1.1083	−0.0928	−0.8586	−2.0841	−0.4291	−1.1583	−1.8891	3.5758	3.3222
HRG-gamma	NM_004495	−3.0435	−2.7642	−3.5591	−3.3918	−3.365	−3.0066	−3.6702	−3.2088	−2.5484	−2.8349	−3.1273	−2.8415	−3.5733	−2.6315	0	0
PARG1	NM_004815	−3.579	−2.8197	−3.3321	−3.4545	−3.6218	−2.678	−2.6794	−3.0388	−3.2966	−2.0305	−3.9068	−3.4694	−3.1961	−2.4445	−1.0763	0
MYCN	NM_005378	−2.7601	−3.6677	−3.7899	−2.5286	−2.7087	−2.7141	−3.2058	−2.4416	−2.1501	−3.3287	−3.329	−3.0585	−3.7126	−3.0375	0	−1.8303
S100A11	NM_005620	−0.7903	−1.5457	−0.8165	−0.6245	−3.1072	−6.1108	−3.2326	−1.5212	−0.8772	−4.9434	−5.8851	−4.0462	−5.5571	−5.0866	−0.621	−0.388
S100A12	NM_005621	−1.8649	−2.5536	−2.3462	−3.3918	−2.2447	−1.863	−2.6611	−3.1148	−1.8131	−1.5468	−2.0481	−2.8415	−2.4389	−1.9388	3.5746	3.8939
SH3BP4	NM_014521	−2.0548	−2.5457	−2.7802	−3.2185	−1.8551	−2.374	−2.9853	−2.6997	−2.8641	−2.6396	−3.1149	−2.7391	−2.5244	−2.7546	0	0
SAMHD1	NM_015474	−1.7555	−2.2633	−2.2307	−2.1326	−2.3417	−3.9735	−4.2737	−3.4173	−2.4362	−1.7002	0.468	−2.6528	−1.6283	−0.3059	1.9357	2.0445
RAI14	NM_015577	−3.1478	−3.5225	−3.1857	−3.1135	−2.6889	0	−3.9079	−2.8007	−1.417	−1.3361	−2.9729	−3.5367	−2.7684	−3.9443	0	0
SH2D4A	NM_022071	−2.0049	−0.9299	−0.4187	−2.8589	−1.6987	−2.111	−2.3374	−1.8217	−1.4284	−0.7936	−1.9068	−2.0161	−1.4771	−1.5014	0	0
MATN2, transcript variant 2	NM_030583	−1.8949	−2.8873	−2.4563	−2.5976	−2.531	−3.1598	−2.5561	−2.2653	−2.4517	−2.2923	−3.1528	−2.5195	−2.4616	−3.4849	0	0
PTPNS1	NM_080792	−2.8748	−1.5575	−3.6787	−2.5118	−2.9697	−1.5791	−2.4194	−2.0954	−1.8081	−2.4922	−2.66	−2.0834	−2.4771	−2.0926	0.6197	0.1952
Similar to TCR delta chain (LOC122700)	XM_058650	−3.1358	−2.0828	−3.0413	−3.2459	−3.0684	−2.9199	−2.7452	−2.9903	−2.3832	−0.412	−2.803	−2.6161	−2.3368	−0.9728	1.3643	1.7152

PEL and high in BL, very low BCL6 in PEL, and very high in BL (Figure 2, Table 2). In addition, very strong expression of IRF4/MUM1 in PEL was characteristic, compared to the other cell lines.

If there are common genes in all tumor cell lines analyzed this time, such genes could be generally required for their establishment and/or maintenance. Thus, we mined the data in such point of view and found a couple of genes were commonly overexpressed compared to normal PBMC (Figure 3, Table 3). It is interesting that these include genes involved in signaling. However, since most of genes are not known well for their function, it remains to be clarified what they do and how important they are.

In the same way, we also mined the data to find less expression in all types of cell line (Table 4), which might give disadvantage to cancer formation and/or maintenance. Actually, we found fifty or so of such genes, most of them are functionally unknown, and detailed analyses will be required in near future (data not shown).

3. Conclusions

Studying gene expression profiles gives us various kinds of information. The analysis especially in cancer will lead to understanding how cancers are generated and maintained and to design what to do in order to suppress cancer growth. It is, however, just screening, and we have much work to do for this aim.

References

[1] P. M. Howly and D. R. Lowy, *Papillomaviruses*, Lippincott Williams & Wilkins, Philadelphia, Pa, USA, 2007.

[2] D. Kremsdorf, P. Soussan, P. Paterlini-Brechot, and C. Brechot, "Hepatitis B virus-related hepatocellular carcinoma: paradigms for viral-related human carcinogenesis," *Oncogene*, vol. 25, no. 27, pp. 3823–3833, 2006.

[3] M. Levrero, "Viral hepatitis and liver cancer: the case of hepatitis C," *Oncogene*, vol. 25, no. 27, pp. 3834–3847, 2006.

[4] M. Matsuoka and K. T. Jeang, "Human T-cell leukaemia virus type 1 (HTLV-1) infectivity and cellular transformation," *Nature Reviews Cancer*, vol. 7, no. 4, pp. 270–280, 2007.

[5] L. S. Young and A. B. Rickinson, "Epstein-Barr virus: 40 years on," *Nature Reviews Cancer*, vol. 4, no. 10, pp. 757–768, 2004.

[6] A. B. Rickinson and E. Kieff, *Epstein-Barr Virus*, Lippincott Williams & Wilkins, Philadelphia, Pa, USA, 2007.

[7] M. Q. Du, H. Liu, T. C. Diss et al., "Kaposi sarcoma-associated herpesvirus infects monotypic (IgMλ) but polyclonal naive B cells in Castleman disease and associated lymphoproliferative disorders," *Blood*, vol. 97, no. 7, pp. 2130–2136, 2001.

[8] D. P. McDonagh, J. Liu, M. J. Gaffey, L. J. Layfield, N. Azumi, and S. T. Traweek, "Detection of Kaposi's sarcoma-associated herpesvirus-like DNA sequences in angiosarcoma," *American Journal of Pathology*, vol. 149, no. 4, pp. 1363–1368, 1996.

[9] D. Ganem, *Kaposi's Sarcoma-Associated Herpesvirus*, Lippincott Williams & Wilkins, Philadelphia, Pa, USA, 2007.

[10] U. R. Hengge, T. Ruzicka, S. K. Tyring et al., "Update on Kaposi's sarcoma and other HHV8 associated diseases. Part 2: pathogenesis, Castleman's disease, and pleural effusion lymphoma," *Lancet Infectious Diseases*, vol. 2, no. 6, pp. 344–352, 2002.

[11] U. R. Hengge, T. Ruzicka, S. K. Tyring et al., "Update on Kaposi's sarcoma and other HHV8 associated diseases. Part 1: epidemiology, environmental predispositions, clinical manifestations, and therapy," *Lancet Infectious Diseases*, vol. 2, no. 5, pp. 281–292, 2002.

[12] P. S. Moore and Y. Chang, "Kaposi's sarcoma-associated herpesvirus immunoevasion and tumorigenesis: two sides of the same coin?" *Annual Review of Microbiology*, vol. 57, pp. 609–639, 2003.

[13] R. Sarid, S. J. Olsen, and P. S. Moore, "Kaposi's sarcoma-associated herpesvirus: epidemiology, virology, and molecular biology," *Advances in Virus Research*, vol. 52, pp. 139–232, 1999.

[14] H. Feng, M. Shuda, Y. Chang, and P. S. Moore, "Clonal integration of a polyomavirus in human Merkel cell carcinoma," *Science*, vol. 319, no. 5866, pp. 1096–1100, 2008.

[15] R. Dalla Favera, S. Martinotti, and R. C. Gallo, "Translocation and rearrangements of the c-myc oncogene locus in human undifferentiated B-cell lymphomas," *Science*, vol. 219, no. 4587, pp. 963–967, 1983.

[16] E. Cesarman and D. M. Knowles, "The role of Kaposi's sarcoma-associated herpesvirus (KSHV/HHV-8) in lymphoproliferative diseases," *Seminars in Cancer Biology*, vol. 9, no. 3, pp. 165–174, 1999.

[17] S. I. Grivennikov, F. R. Greten, and M. Karin, "Immunity, inflammation, and cancer," *Cell*, vol. 140, no. 6, pp. 883–899, 2010.

[18] D. Elgui de Oliveira, "DNA viruses in human cancer: an integrated overview on fundamental mechanisms of viral carcinogenesis," *Cancer Letters*, vol. 247, no. 2, pp. 182–196, 2007.

[19] B. Damania, "Oncogenic γ-herpesviruses: comparison of viral proteins involved in tumorigenesis," *Nature Reviews Microbiology*, vol. 2, no. 8, pp. 656–668, 2004.

[20] H. Varmus, "Retroviruses," *Science*, vol. 240, no. 4858, pp. 1427–1435, 1988.

[21] Y. Chang, E. Cesarman, M. S. Pessin et al., "Identification of herpesvirus-like DNA sequences in AIDS-associated Kaposi's sarcoma," *Science*, vol. 266, no. 5192, pp. 1865–1869, 1994.

[22] J. J. Russo, R. A. Bohenzky, M. C. Chien et al., "Nucleotide sequence of the Kaposi sarcoma-associated herpesvirus (HHV8)," *Proceedings of the National Academy of Sciences of the United States of America*, vol. 93, no. 25, pp. 14862–14867, 1996.

[23] A. Potthoff, N. H. Brockmeyer, M. Stucker, U. Wieland, A. Kreuter, and H. A. Competence Network, "Kaposi sarcoma in a HIV uninfected man who has sex with men," *European Journal of Medical Research*, vol. 15, no. 2, pp. 79–80, 2010.

[24] C. Boshoff and R. A. Weiss, "Kaposi's sarcoma-associated herpesvirus," *Advances in Cancer Research*, vol. 75, pp. 57–86, 1998.

[25] P. P. Naranatt, H. H. Krishnan, S. R. Svojanovsky, C. Bloomer, S. Mathur, and B. Chandran, "Host gene induction and transcriptional reprogramming in kaposi's sarcoma-associated herpesvirus (KSHV/HHV-8)-infected endothelial, fibroblast, and B cells: insights into modulation events early during infection," *Cancer Research*, vol. 64, no. 1, pp. 72–84, 2004.

[26] K. Ueda, S. Sakakibara, E. Ohsaki, and K. Yada, "Lack of a mechanism for faithful partition and maintenance of the KSHV genome," *Virus Research*, vol. 122, no. 1-2, pp. 85–94, 2006.

[27] L. Arvanitakis, E. A. Mesri, R. G. Nador et al., "Establishment and characterization of a primary effusion (body cavity-based) lymphoma cell line (BC-3) harboring Kaposi's sarcoma-associated herpesvirus (KSHV/HHV-8) in the absence of Epstein-Barr virus," *Blood*, vol. 88, no. 7, pp. 2648–2654, 1996.

[28] K. Nishimura, K. Ueda, S. Sakakibara et al., "Functional analysis of Kaposi's sarcoma-associated herpesvirus RTA in an RTA-depressed cell line," *Journal of Human Virology*, vol. 4, no. 6, pp. 296–305, 2001.

[29] N. Shimizu, A. Tanabe-Tochikura, Y. Kuroiwa, and K. Takada, "Isolation of Epstein-Barr virus (EBV)-negative cell clones from the EBV- positive Burkitt's lymphoma (BL) line Akata: malignant phenotypes of BL cells are dependent on EBV," *Journal of Virology*, vol. 68, no. 9, pp. 6069–6073, 1994.

[30] K. Ueda, E. Ito, M. Karayama, E. Ohsaki, K. Nakano, and S. Watanabe, "KSHV-infected PEL cell lines exhibit a distinct gene expression profile," *Biochemical and Biophysical Research Communications*, vol. 394, no. 3, pp. 482–487, 2010.

[31] H. Katano, Y. Hoshino, Y. Morishita et al., "Establishing and characterizing a CD30-positive cell line harboring HHV-8 from a primary effusion lymphoma," *Journal of Medical Virology*, vol. 58, no. 4, pp. 394–401, 1999.

[32] R. Renne, W. Zhong, B. Herndier et al., "Lytic growth of Kaposi's sarcoma-associated herpesvirus (human herpesvirus 8) in culture," *Nature Medicine*, vol. 2, no. 3, pp. 342–346, 1996.

[33] E. Cesarman, P. S. Moore, P. H. Rao, G. Inghirami, D. M. Knowles, and Y. Chang, "In vitro establishment and characterization of two acquired immunodeficiency syndrome-related lymphoma cell lines (BC-1 and BC-2) containing Kaposi's sarcoma-associated herpesvirus-like (KSHV) DNA sequences," *Blood*, vol. 86, no. 7, pp. 2708–2714, 1995.

[34] K. Takada, K. Horinuchi, Y. Ono et al., "An Epstein-Barr virus-producer line Akata: establishment of the cell line and analysis of viral DNA," *Virus Genes*, vol. 5, no. 2, pp. 147–156, 1991.

[35] B. Herndier and D. Ganem, "The biology of Kaposi's sarcoma," *Cancer Treatment and Research*, vol. 104, pp. 89–126, 2001.

[36] S. A. Miles, "Kaposi sarcoma: a cytokine-responsive neoplasia?" *Cancer Treatment and Research*, vol. 63, pp. 129–140, 1992.

[37] H. W. Wang, M. W. B. Trotter, D. Lagos et al., "Kaposi sarcoma herpesvirus-induced cellular reprogramming contributes to the lymphatic endothelial gene expression in Kaposi sarcoma," *Nature Genetics*, vol. 36, no. 7, pp. 687–693, 2004.

[38] Y. K. Hong, K. Foreman, J. W. Shin et al., "Lymphatic reprogramming of blood vascular endothelium by Kaposi sarcoma-associated herpesvirus," *Nature Genetics*, vol. 36, no. 7, pp. 683–685, 2004.

[39] M. Weinreb, P. J. Day, F. Niggli et al., "The role of Epstein-Barr virus in Hodgkin's disease from different geographical areas," *Archives of Disease in Childhood*, vol. 74, no. 1, pp. 27–31, 1996.

[40] L. L. Decker, P. Shankar, G. Khan et al., "The Kaposi sarcoma-associated herpesvirus (KSHV) is present as an intact latent genome in KS tissue but replicates in the peripheral blood mononuclear cells of KS patients," *Journal of Experimental Medicine*, vol. 184, no. 1, pp. 283–288, 1996.

[41] J. Chen, K. Ueda, S. Sakakibara, T. Okuno, and K. Yamanishi, "Transcriptional regulation of the Kaposi's sarcoma-associated herpesvirus viral interferon regulatory factor gene," *Journal of Virology*, vol. 74, no. 18, pp. 8623–8634, 2000.

[42] K. Yada, E. Do, S. Sakakibara et al., "KSHV RTA induces a transcriptional repressor, HEY1 that represses rta promoter," *Biochemical and Biophysical Research Communications*, vol. 345, no. 1, pp. 410–418, 2006.

[43] A. Chadburn, E. M. Hyjek, W. Tam et al., "Immunophenotypic analysis of the Kaposi sarcoma herpesvirus (KSHV; HHV-8)-infected B cells in HIV+ multicentric Castleman disease (MCD)," *Histopathology*, vol. 53, no. 5, pp. 513–524, 2008.

[44] E. Oksenhendler, M. Duarte, J. Soulier et al., "Multicentric Castleman's disease in HIV infection: a clinical and pathological study of 20 patients," *Aids*, vol. 10, no. 1, pp. 61–67, 1996.

[45] D. Dittmer, C. Stoddart, R. Renne et al., "Experimental transmission of kaposi's sarcoma-associated herpesvirus (KSHV/HHV-8) to SCID-hu Thy/Liv mice," *Journal of Experimental Medicine*, vol. 190, no. 12, pp. 1857–1868, 1999.

[46] T. S. Uldrick, V. Wang, D. O'Mahony et al., "An interleukin-6-related systemic inflammatory syndrome in patients co-infected with kaposi sarcoma-associated herpesvirus and HIV but without multicentric castleman disease," *Clinical Infectious Diseases*, vol. 51, no. 3, pp. 350–358, 2010.

[47] C. Parravicini, B. Chandran, M. Corbellino et al., "Differential viral protein expression in Kaposi's sarcoma-associated herpesvirus-infected diseases: Kaposi's sarcoma, primary effusion lymphoma, and multicentric Castleman's disease," *American Journal of Pathology*, vol. 156, no. 3, pp. 743–749, 2000.

[48] R. Hamoudi, T. C. Diss, E. Oksenhendler et al., "Distinct cellular origins of primary effusion lymphoma with and without EBV infection," *Leukemia Research*, vol. 28, no. 4, pp. 333–338, 2004.

[49] A. Matolcsy, R. G. Nador, E. Cesarman, and D. M. Knowles, "Immunoglobulin V(H) gene mutational analysis suggests that primary effusion lymphomas derive from different stages of B cell maturation," *American Journal of Pathology*, vol. 153, no. 5, pp. 1609–1614, 1998.

[50] R. Kuppers, "Mechanisms of B-cell lymphoma pathogenesis," *Nature Reviews Cancer*, vol. 5, no. 4, pp. 251–262, 2005.

[51] R. Taub, I. Kirsch, and C. Morton, "Translocation of the c-myc gene into the immunoglobulin heavy chain locus in human Burkitt lymphoma and murine plasmacytoma cells," *Proceedings of the National Academy of Sciences of the United States of America*, vol. 79, no. 24, pp. 7837–7841, 1982.

[52] F. Baran-Marszak, R. Fagard, B. Girard et al., "Gene array identification of Epstein Barr virus-regulated cellular genes in EBV-converted Burkitt lymphoma cell lines," *Laboratory Investigation*, vol. 82, no. 11, pp. 1463–1479, 2002.

[53] J. Yuan, E. Cahir-McFarland, B. Zhao, and E. Kieff, "Virus and cell RNAs expressed during Epstein-Barr virus replication," *Journal of Virology*, vol. 80, no. 5, pp. 2548–2565, 2006.

Biochemical and Biophysical Research Communications 394 (2010) 482–487

Contents lists available at ScienceDirect

Biochemical and Biophysical Research Communications

journal homepage: www.elsevier.com/locate/ybbrc

KSHV-infected PEL cell lines exhibit a distinct gene expression profile

Keiji Ueda [a,*], Emi Ito [b], Masato Karayama [c], Eriko Ohsaki [a], Kazushi Nakano [a], Shinya Watanabe [b]

[a] Division of Virology, Department of Microbiology and Immunology, Osaka University Graduate School of Medicine, 2-2 Yamada-oka, Suita, Osaka 565-0871, Japan
[b] Department of Clinical Genomics, Translational Research Center, Fukushima Medical University, Hikarigaoka-1, Fukushima 960-1295, Japan
[c] Department of Infectious Diseases, Hamamatsu University School of Medicine, 1-20-1 Handayama, Higashi-ku, Hamamatsu, Shizuoka 431-3192, Japan

ARTICLE INFO

Article history:
Received 12 February 2010
Available online 20 February 2010

Keywords:
Kaposi's sarcoma-associated herpesvirus
Primary effusion lymphoma
Epstein–Barr virus
Burkitt lymphoma
T-cell lymphoma
DNA chip

ABSTRACT

We analyzed the gene expression profiles of lymphocyte-originated tumor cell lines – primary effusion lymphoma (PEL) cell lines, T-cell leukemia (TCL) cell lines, Burkitt lymphoma (BL) cell lines – and two sets of normal peripheral blood mononuclear cells (PBMCs) – in order to determine characteristic gene expression profiles for each of the former three groups. And we found that these cell lines showed respective typical gene expression profiles and classified into clear four groups, PEL, TCL, BL, and normal PBMCs. Two B lymphocyte-originated tumor cell lines, PEL and BL cell lines, clearly exhibited distinct gene expression profiles, respectively. Even though there was only one line that was co-infected with both Kaposi's sarcoma-associated herpesvirus (KSHV) and Epstein–Barr virus (EBV), KSHV seemed to govern the gene expression profile of the co-infected line. These data suggested not only that established typical tumor cell lines show a distinct gene expression profile but also that this profile may be governed by certain viruses.

1. Introduction

Kaposi's sarcoma-associated herpesvirus (KSHV) or human herpesvirus 8 (HHV-8) was discovered in AIDS-associated Kaposi's sarcoma [1] and established as an etiologic agent for all forms of this disease [2]. KSHV is also found in almost all of two B cell lymphomas, primary effusion lymphoma (PEL) [3], and plasmablastic lymphoma associated with multicentric Castleman's disease [4]. PEL typically presents as a lymphomatous effusion in the pleural/peritoneal cavity without forming a solid mass [5].

Epstein–Barr virus (EBV), another human gamma-herpesvirus, is well known as an etiological agent of many types of cancer originated from T and B cell lymphocytes as well as gastric cancer [6]. Typical EBV-associated tumors are Burkitt lymphomas and classical Hodgkin's lymphomas, both of which are originated from B lymphocytes [7]. Although PEL often co-infects both with KSHV and EBV, KSHV seems to be primarily responsible for the transformation [5,8].

The advent of DNA microarray technology has been very helpful for revealing the characteristic profiles of transcriptomes of tissues including cancers. There have been many reports showing how infections with various viruses, including KSHV and EBV, affect cellular gene expression profiles [9]. Here, we analyzed the gene expression profiles of cell lines established from human lymphocytic leukemia. These were KSHV-infected primary effusion lymphoma (PEL) cell lines, either EBV-infected and non-infected Burkitt lymphoma (B-L) cell lines and several T-cell lymphoma (TCL) cell lines, including two sets of normal human peripheral mononuclear cells (PBMCs). Each of these groups showed a clearly distinguishable gene expression profile. The results suggested not only that a typical tumor cell type shows a distinct gene expression pattern but also that the gene expression profile of a typical tumor cell line seems to be governed by some virus infection.

2. Materials and methods

2.1. Cells and RNA

The PEL cell lines used were TY1 [10], BCBL1 [11], D90 which was a derivative of BCBL1 and not inducible for lytic replication by tetradecanoylphorbol 13-acetate (TPA) [12], BC3 [13], and BC1 [14]. All these cell lines are latently infected with KSHV and only BC1 is co-infected with KSHV and EBV, and they were cultured in the RPMI1640 medium (Wako Chemicals, Osaka, Japan) containing 20% heat-inactivated fetal bovine serum (FBS), 10 i.u. per ml penicillin G and 10 μg per ml streptomycin under a 5% CO_2 atmosphere. The BL cell lines used were Ramos, BJAB, Daudi, Akata which was the gift of Dr. Takada, Hokkaido University [15], and Raji. For the RT-PCR (see below), Namalwa, an EBV-positive Burkitt lymphoma cell line and MC116, which is an undifferentiated B cell lymphoma cell line, were also utilized. All these cell lines were infected with EBV except Ramos, BJAB and MC116, and the EBV genomes in Raji and in Daudi cells were found to be defective [16,17]. Several TCL

* Corresponding author. Fax: +81 6 6879 3789.
E-mail address: kueda@virus.med.osaka-u.ac.jp (K. Ueda).

0006-291X/$ - see front matter © 2010 Elsevier Inc. All rights reserved.
doi:10.1016/j.bbrc.2010.02.122

cell lines were also analyzed: Jurkat (an acute T-cell leukemia), Molt-3 (an acute T lymphoblastic leukemia), SupT1 (a T lymphoblastic leukemia) and MT4 (an adult T-cell leukemia cell line). Among them, only MT4 contained integrated retroviral genomes of human T-cell leukemia virus-1 (HTLV-1). The BL and TCL cell lines were cultured under the same condition except 10% heat-inactivated FBS was used in place of 20% heat-inactivated FBS. Samples were prepared as either a TPA-induced or non-induced version for all cell lines. RNA was extracted from these cells three times, when the cells grew to 1×10^6/ml in the 25 ml culture medium. When cells were induced by TPA, TPA was added into medium at 1×10^6/ml cell density and left for 48 h. The cells under this condition were pelleted and lysed with 5 ml Trizol® (Invitrogen, Carlsbad, CA). The solution was stored at 4 °C refrigerator until the other preparation was completed. Finally, three lysed solutions were combined and the total RNA was extracted.

For RNA preparation of the healthy candidates peripheral blood mononuclear cells (PBMCs) of two healthy volunteers, 20 ml of venous blood was obtained in a 100 U heparin containing syringe and spun down at 1500*g* for 15 min at room temperature [18]. The plasma was discarded and an equal volume of 0.02% EDTA–phosphate buffered saline (−) (PBS [−]) was added. The mixed blood was layered on a 20 ml Ficoll-Paque (GE Healthcare, Buckinghamshire, UK) and centrifuged at 1500*g* for 3 min at RT. Banded PBMCs were collected, suspended in three volumes of 0.02% EDTA–PBS (−) and pelleted at 1500*g* for 3 min at RT. The supernatant was carefully and completely discarded and 5 ml Trizol® (Invitrogen) was added. The samples were prepared three times and all preparations were combined finally.

Total RNA was extracted from the lysate according to the manufacturer's instructions. Poly(A)$^+$ RNA was purified from the total RNA using a MicroPoly(A)Purist™ Kit (Ambion, Austin, TX) according to the manufacturer's instructions. The purified poly(A)$^+$ RNA was divided into aliquots of 2.0 μg, precipitated with ethanol, and stored at −20 °C.

2.2. Microarray hybridization and data analysis

Synthetic polynucleotides of 80 mer representing 30,913 species of human transcripts (MicroDiagnostic, Tokyo, Japan) were printed on a glass slide using a custom-made arrayer. The aliquots of 2.0-μg RNA were subjected to first-strand cDNA synthesis in the presence of Cyanine-5 dUTP (PerkinElmer, Boston, MA) for samples obtained from the cell lines or Cyanine-3 dUTP (PerkinElmer) for a human common reference RNA in a reaction mixture derived from a labeling and hybridization kit (MicroDiagnostic). The human common reference RNA was prepared by mixing equal amounts of poly(A)$^+$ RNA extracted from 22 human cancer cell lines to reduce cell type-specific bias of expression. The red fluorescence-labeled cDNA of the samples and the green fluorescence-labeled common reference RNA were equally mixed and hybridized to a microarray. The hybridized microarray was washed with the labeling and hybridization kit and subsequently scanned by using a GenePix 4000A scanner (Axon Instruments, Union City, CA). Fluorescence signals were detected and processed by GenePix Pro 3.0 software (Axon Instruments). The processed raw data (median of ratios) were normalized by multiplying with the normalization factors provided in the GenePix Pro 3.0 software package. The normalized data (expression ratios) were converted into $\log_2$ values (designated log ratios).

2.3. Reverse transcription followed by PCR (RT-PCR) and quantitative RT-PCR (q-PCR)

Cells were cultured and the total RNA was extracted under the same conditions described above for the RNA preparation as mentioned. Ten micrograms total RNA was subjected to cDNA synthesis with a first-strand synthesis kit (Roche, Mannheim, Germany). The one-twentieth (~0.5 μg RNA equivalent) was used for RT-PCR and q-PCR. In this report, we focused on the angiopoietin-1 (*ang-1*) gene and prepared the following primers to detect its expression:

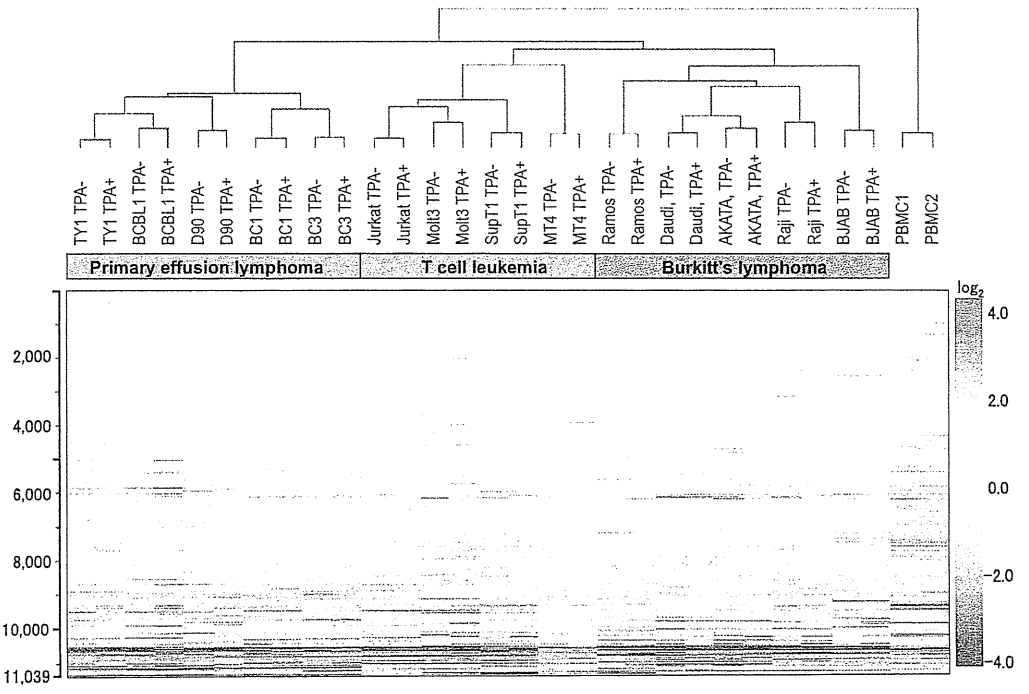

Fig. 1. Cluster analysis of the PEL, TCL, and BL cell lines. The expression levels of about 30,000 genes in each of the cell lines were analyzed with a DNA chip. The cluster analysis revealed that each category of tumor cell lines showed a distinct expression profile, and in most of cases TPA induction did not grossly change the expression profile.

Angpt1-FW1, 5′-TTCCTCGCTGCCATTCTGACTC-3′ and Angpt1-RV1, 5′-GGTGGATAATGAATTCTCCAGC. PCR was performed at 95 °C for 30 s, 54 °C for 30 s and 72 °C for 1 min with Ex-Taq® polymerase (Takara, Tokyo, Japan). This reaction generated about an approximately 480-bp fragment, which was cloned into a bluescript II vector (Stratagene, La Jolla, CA) to set the standards for q-PCR. q-PCR was performed with Roche's LightCycler FastStart DNA Master SYBR Green I according to the manufacture's instructions.

3. Results and discussion

3.1. KSHV-infected PEL cell lines show distinct gene expression profiles

In this analysis, we tried to determine whether KSHV-infected PEL cells showed different gene expression patterns different from those of several other cell lines, especially from BL cell lines, since both were originated from the B cell lineage. A previous report suggested that PEL cells resemble transformed postgerminal center (GC) B cells, although some PELs have been reported to be of pre-GC origin [5] and BL cells have been reported to resemble GC B cells [19]. For this purpose, we utilized a DNA microarray analysis. We prepared three different types of lymphatic tumor cell lines and normal peripheral blood mononuclear cells – PEL cell lines (TY1, BCBL1, BC1, BC3, and D90, a derivative of BCBL1), T-cell lymphoma cell lines (SupT1, Jurkat, Molt3, and MT4) and BL cell lines (BJAB, Daudi, Ramos, Raji, and Akata) – as well as two PBMC sets. All of the PEL cell lines were infected with KSHV, but only BC1 was co-infected with KSHV and EBV. In the case of the BL cell lines, all but BJAB and Ramos were infected with EBV. About 30,000 genes were analyzed on the DNA chip. The analysis was normalized with the human common reference RNA (see Section 2), which means that the average gene expression was shown to be around zero by the value of $\log_2$.

The results showed a clear difference of gene expression profiles between the PEL, TCL, and BL cell lines, i.e., each cell line was categorized into a distinct group (Fig. 1). Thus, even though PEL and BL were originated from B cells, their gene expression profiles were quite characteristic. In almost all cases, PEL was indeed infected with KSHV and frequently co-infected with EBV. Actually, PEL cell lines were established with KHSV and EBV co-infected status, but EBV frequently disappeared during in vitro culturing in vitro at least [10,11,13,20–23]. This phenomenon strongly suggests that KSHV could have an important role for maintenance of the PEL cell lines in vitro and probably governs the gene expression profile. Indeed, the KSHV genome appeared to be stringently maintained in terms of the copy number and never disappeared, whereas the EBV genome was easily lost and EBV-negative cell lines could be established from original EBV-positive BL cell lines [15]. Though there was only one cell line (BC1) that was co-infected with KSHV and EBV in this analysis, this expression profile was categorized

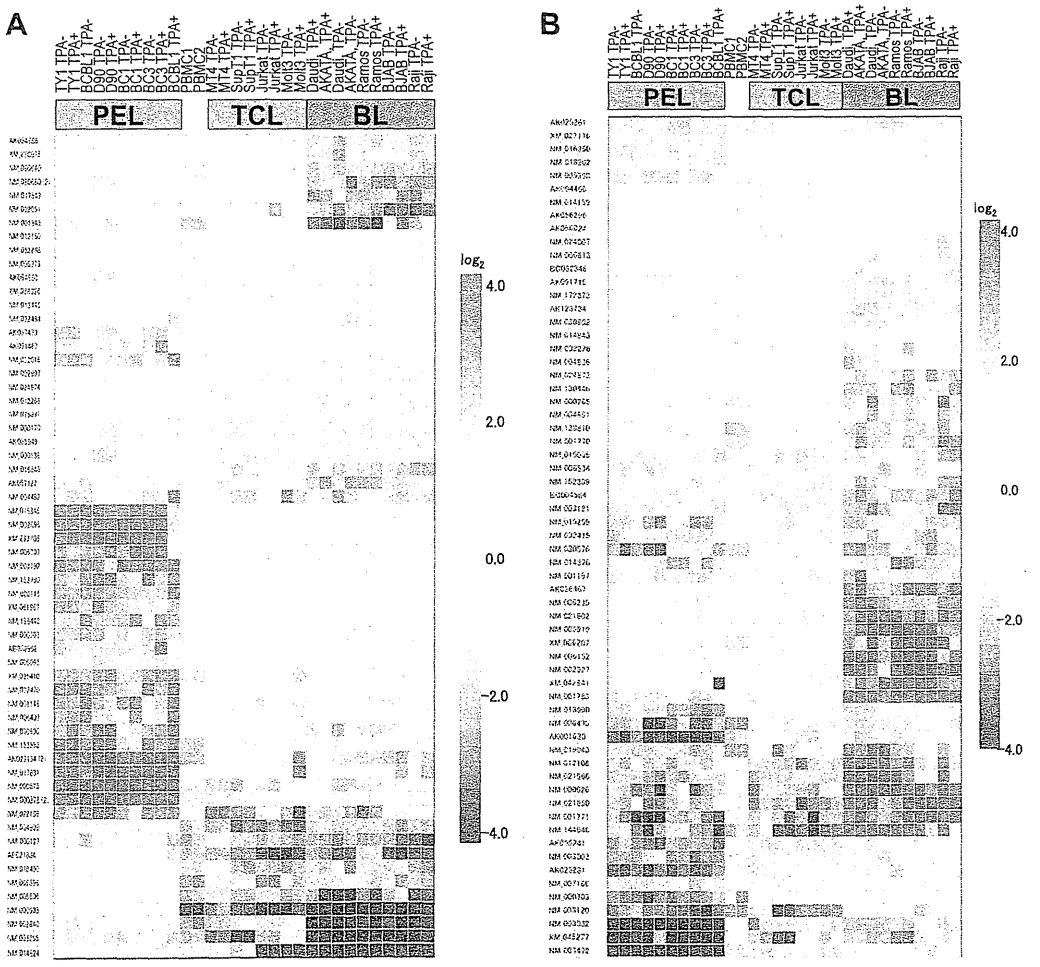

Fig. 2. Genes that were differentially expressed among the PEL, TCL, and BL cell lines. (A) Genes that showed a fourfold higher expression level in PEL cell lines compared with the TCL or BL cell lines. (B) Genes that showed fourfold lower expression level in the PEL cell lines compared with the TCL or BL cell lines. TPA induction on BCBL1 repositioned its profile by cluster analysis, suggesting that TPA had a different effect on each cell line.

into the PEL cluster, which was consistent with a previous report [19].

TPA is often used to reactivate KSHV lytic replication and the effect of TPA on cellular gene expression was also analyzed. Though TPA has a dramatic effect on the viral gene expression [24–26], in this study the drug generally did not change the cellular gene expression profiles (Fig. 1). However, TPA had a slightly different effect on BCBL1 than on the expression profiles of the other cell lines (Fig. 2A and B).

3.2. Characteristic gene expression

We extracted genes whose expression was higher or lower in the PEL cell lines compared with the other clusters. In this analysis, there were 124 genes that showed different expression levels among the three groups and half of them were expressed at relatively higher and lower levels in the PEL cell lines, respectively. Typically, methyl-CpG binding domain protein (NM_015845) (GenBank accession number), RNA polymerase II (NM_002696), tumor necrosis superfamily member (NM_002696), and so on were expressed more highly in the PEL cell lines than in the TCL or BL cell lines (Fig. 2A).

Sialyltransferase 1 (NM_003032), DEK oncogene (NM_003472), Amyloid beta (A4) precursor protein-binding factor (NM_019043), CD79B (NM_000626), and so on seemed to be expressed at lower levels in the PEL lines, and at the higher levels in the BL cell lines (Fig. 2B). CD19, CD22, and CD79A and B, which are typical markers for B cell lineage, were expressed the higher in BL cell lines (Fig. 2B), suggesting that PEL and BL had different characteristics though they were thought to be originated from B cell lineage because of the rearrangement of the immunoglobulin genes [3,27,28]. In the case of many of the genes that showed higher or lower expression in one or another of these cell lines, the function of these expression differences remains to be clarified in terms of their function to give characteristic features to the cell lines.

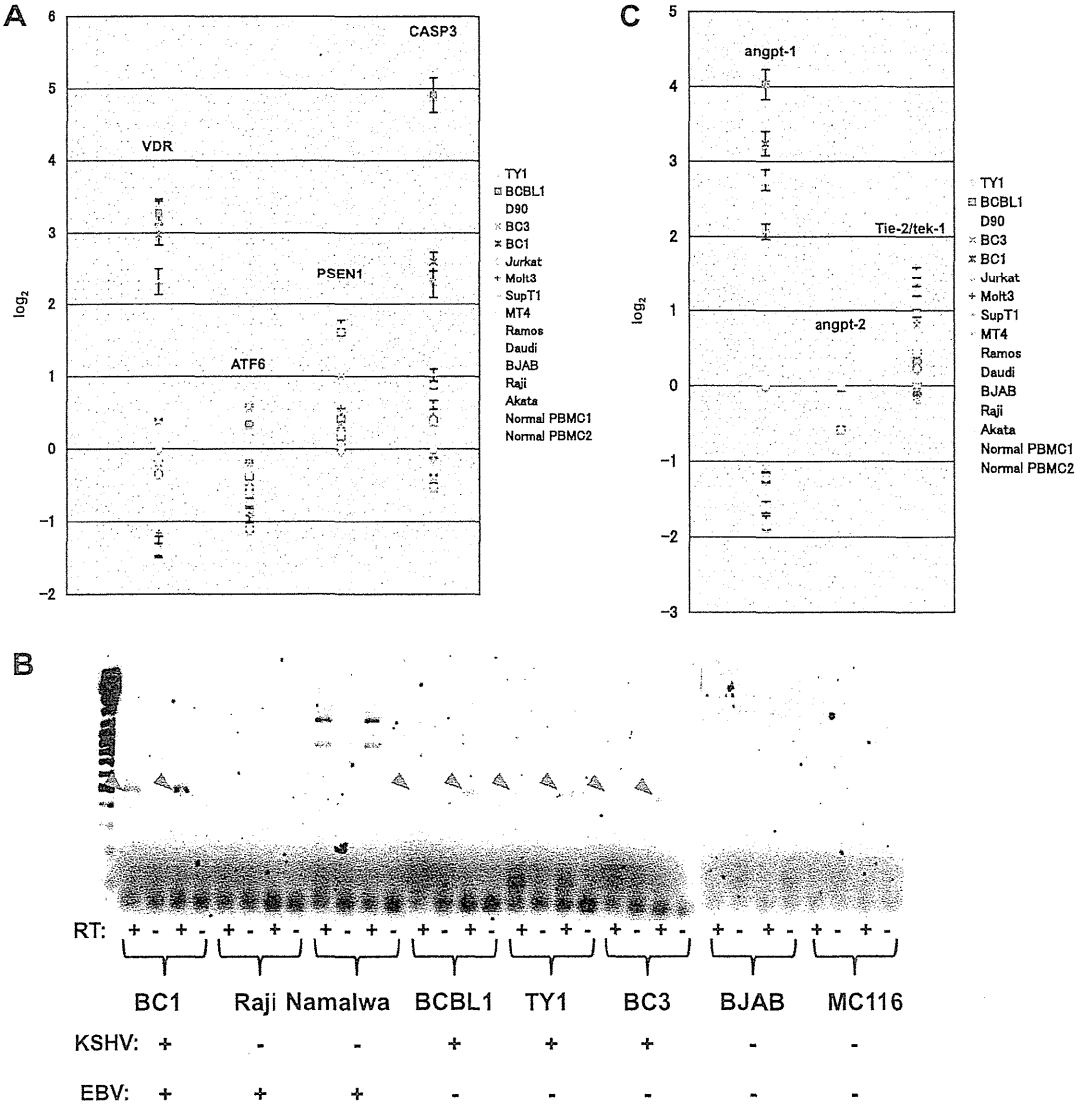

Fig. 3. The expression level of typical genes. (A) Vitamin D (1,25-dihydroxyvitamin D3) receptor (VDR) (NM_01466), caspase 3 (CASP3) (NM_004346), activating transcription factor 6 (ATF6) (NM_005171), and presenilin 1 (Alzheimer disease 3) (PSEN1) (NM_007319) have been reported to be expressed more highly in PEL cell lines than in TCL or BL cell lines. VDR and CASP3, but not ATF6 and PSEN1 were indeed expressed more highly in the PEL cell lines than in the others. (B) In our analysis, only *ang-1* was extremely expressed at high levels in the PEL cell lines while neither *ang-2* nor *Tie-2/tek-1*, which is a receptor gene for *ang-1* and *ang-2*, appeared to be up-regulated. (C) RT-PCR confirmed the higher expression of *ang-1* in the PEL cell lines. *Ang-1* gene expression was detectable level in all the PEL cell lines but not in the TCL or BL cell lines, by RT-PCR. A shorter band was detected in the Raji cell line, the details of which were unclear.